

Amplitude analysis of reaction $\pi^+ n \uparrow \rightarrow \pi^+ \pi^- p$ at 5.98 and 11.85 GeV/c

M. Svec

*Physics Department, Dawson College, Montreal, Quebec, Canada H3Z 1A4
and McGill University, Montreal, Quebec, Canada H3A 2T8*

A. de Lesquen and L. van Rossum*

*Département de Physique des Particules Élémentaires, Centre d'Études Nucléaires,
Saclay, France*

(Received 4 March 1991)

We present a model independent amplitude analysis of reaction $\pi^+ n \uparrow \rightarrow \pi^+ \pi^- p$ at 5.98 and 11.85 GeV/c using Saclay data obtained with a transversely polarized deuteron target at the CERN Proton Synchrotron. The analysis makes use of the data in two sets of binnings to examine the dependence of amplitudes on momentum transfer t [$-t \leq 1.0$ (GeV/c)²] in the ρ^0 mass region and their dependence on dipion mass below 1000 MeV for momentum transfers $-t = 0.2-0.4$ (GeV/c)². The analysis is performed in both t -channel and s -channel helicity frames of the dimeson state and it is verified by comparison with linear bounds on the moduli. The data yield two solutions for 8 moduli and 6 cosines of relative phases of nucleon transversity amplitudes with dimeson spin $J=0$ (S wave) and $J=1$ (P wave). The two solutions differ mainly in the S -wave contributions. Both solutions require nonzero nucleon helicity-nonflip amplitudes (A_1 exchange) with phases different from phases of nucleon helicity-flip amplitudes (π exchange). Natural exchange amplitudes (A_2 exchange) with opposite nucleon transversities show a crossover in their t dependence at $-t_c = 0.4-0.5$ (GeV/c)² which has not been observed in the earlier amplitude analysis of $\pi^- p \uparrow \rightarrow \pi^- \pi^+ n$ at 17.2 GeV/c. We suggest this difference may signal the influence of composite structure of hadrons and nonperturbative QCD effects in pion production. Although the mass dependence of partial-wave cross sections averaged over nucleon spins is smooth, we observe large and systematic structures in moduli squared of nucleon transversity amplitudes which reveal the essential role of nucleon spin in the pion production process. This behavior of moduli does not support the hypothesis of factorization of mass and t dependence of production amplitudes previously used in studies of meson-meson scattering. The mass dependence of S -wave amplitudes suggests the existence of a scalar state $I=0$ $0^{++}(750)$ with a width of 100–150 MeV. Our results emphasize the need for a systematic study of pion production on the level of amplitudes in a new generation of dedicated experiments with spin at the recently proposed high-intensity hadron facilities.

PACS number(s): 13.75.Gx, 13.85.Hd, 13.88.+e

I. INTRODUCTION

The idea to construct scattering amplitudes from data obtained in measurements using polarized targets, polarized beams, and recoil nucleon rescattering was first proposed [1,2] by Bethe in 1958. Such experimental acquisition of scattering amplitudes is known as amplitude analysis. It provides model-independent information about the t structure of amplitudes, their dependence on energy, spin states of particles, etc. The first amplitude analysis [3–6] was possible for two-body scattering, namely, in $\pi N \rightarrow \pi N$ at 6 GeV/c. It allowed an isolation of ρ -exchange amplitudes which showed unexpected structures in their dependence on momentum transfer. This information led to major revisions of Regge models. Later measurements of polarization in $K^+ n \rightarrow K^0 p$ at 6 GeV/c allowed the first construction of A_2 exchange amplitudes in KN two-body scattering [7,8], which also

showed an unexpected behavior. Similarly motivated experiments with polarized proton beams enabled amplitude analyses of nucleon-nucleon two-body scattering [9,10], also at 6 GeV/c. These important experimental results prompted new developments of spin formalism to describe and analyze complete measurements, e.g., in pion photoproduction [11] and NN scattering [12,13]. Of particular interest became the study of optimal spin experiments [14].

In 1964, Gottfried and Jackson pointed out that measurements of angular correlations of particles produced in multiparticle production processes provided direct information about the particle production mechanism [15]. In 1978, Lutz and Rybicky showed [16] that in a single experiment, $\pi N \uparrow \rightarrow \pi \pi N$ or $KN \uparrow \rightarrow K \pi N$ on a transversely polarized target, the measured spin-density-matrix (SDM) elements describing the produced dimeson state provide enough observables for performing an almost complete amplitude analysis in the kinematic region where the produced dimeson state has total angular momentum $J=0$ (S wave) and $J=1$ (P wave). Experimentally, the pion production is dominated by S - and P -wave dimeson states for dimeson masses $m \lesssim 1000$ MeV.

*Present address: Fermilab, P. O. Box 500, Batavia, IL 60510.

For higher invariant masses, the dimeson states with $J=2$ (D wave) and higher angular momentum are important contributions. The increase in the number of production amplitudes renders the amplitude analysis somewhat model dependent when only data on transversely polarized targets are available [16].

The first measurement of the reaction $\pi^- p \uparrow \rightarrow \pi^- \pi^+ n$ on a polarized target was done at CERN at 17.2 GeV/c. The data enabled a model-independent amplitude analysis in two kinematic regions of momentum-transfer squared $-t$ and dipion mass m , looking at the momentum-transfer dependence of amplitudes in ρ^0 mass region [17,18],

$$0 \leq -t \leq 1.0 \text{ (GeV/c)}^2 \text{ with } m = 710\text{--}830 \text{ MeV}, \quad (1.1)$$

and at their mass dependence [17–20] at small t :

$$600 \leq m \leq 900 \text{ MeV with } -t = 0.005\text{--}0.2 \text{ (GeV/c)}^2. \quad (1.2)$$

Model-dependent analyses with contributions from higher spin states were also performed for higher masses [19,20] $900 \leq m \leq 1780$ MeV at small $-t \leq 0.2$ (GeV/c)² as well as at larger momentum transfers [20–23]. The results provided evidence for significant contributions from helicity-nonflip amplitudes with A_1 exchange quantum numbers ($J^G=1^-, J^{PC}=1^{++}$) which had long been assumed to be absent and suggested a possible existence of non- $q\bar{q}$ meson states [20–23]. Evidence for A_1 exchange came independently also from amplitude analyses of nucleon-nucleon two-body scattering [9,10]. The importance of A_1 exchange in nucleon-nucleon scattering was theoretically anticipated earlier by Blackman and Goldstein [24].

The first measurement of $\pi^+ n \uparrow \rightarrow \pi^+ \pi^- p$ on a polarized deuteron target was done at 5.98 and 11.85 GeV/c at CERN by the Saclay group [25–30]. The experiment covered the kinematic region of $0.10 \leq -t \leq 1.0$ (GeV/c)² and $360 \leq m \leq 1040$ MeV. Average values of 14 normalized S - and P -wave spin-density-matrix elements were obtained [28,30] in four sets of (m, t) binnings in both s - and t -channel dipion helicity frames [31]. The first two sets

$$0.1 \leq -t \leq 1.0 \text{ (GeV/c)}^2 \text{ with } m = 720\text{--}820 \text{ MeV} \quad (1.3)$$

and

$$360 \leq m \leq 1040 \text{ MeV with } -t = 0.2\text{--}0.4 \text{ (GeV/c)}^2 \quad (1.4)$$

provide information about the t dependence of pion production in the ρ^0 mass region and about its dependence on dipion mass in the interval of larger momentum transfers as compared to (1.2). The other two sets of binnings cover broader region of m and t , allowing the study of the t evolution of mass dependence of measured observables and amplitudes.

In this report we present the results of model-independent amplitude analysis of the Saclay data for $\pi^+ n \uparrow \rightarrow \pi^+ \pi^- p$ at 5.98 and 11.85 GeV/c in the (m, t) binnings (1.3) and (1.4) in both s - and t -channel dipion helicity frames. Preliminary results [32,33], tables with final results [34], and partial results [35–38] were published earlier elsewhere.

The paper is organized in six sections. The kinematics, observables, and pion production amplitudes are introduced in Sec. II. The method of amplitude analysis is described in Sec. III. In Sec. IV we present our results and verify our analysis in comparison with linear bounds on the moduli. In Sec. V we discuss a Regge model for t dependence in ρ^0 mass region, factorization hypothesis for m dependence of amplitudes, and possible effects of hadron structure. The Appendix describes the method for calculation of relative phases between natural and unnatural exchange amplitudes. Section VI closes the paper with a summary.

II. BASIC FORMALISM

A. Kinematics

The kinematical variables used to describe the dimeson production on a polarized nucleon target at rest are $(s, t, m, \theta, \varphi, \psi, \delta)$ [39,40]. Here s is the center-of-mass-system energy squared, t is the four-momentum-transfer squared, and m is the $\pi^+ \pi^-$ invariant mass. The angles (φ, θ) describe the direction of the π^+ in the $\pi^+ \pi^-$ rest frame. The angles (ψ, δ) describe the direction of the target nucleon polarization \mathbf{P} in the target nucleon rest frame. The angle ψ is the angle between the direction of the transverse component of target polarization, \mathbf{P}_T , and the normal \mathbf{n} to the production plane [29]. The angle δ is the angle between the target polarization \mathbf{P} and its transverse component \mathbf{P}_T with respect to the incident momentum [29]. The direction of normal \mathbf{n} is defined according to the Basel convention by $\mathbf{p}_\pi \times \mathbf{p}_{\pi\pi}$, where \mathbf{p}_π and $\mathbf{p}_{\pi\pi}$ are the incident pion and dimeson momenta in the target neutron rest frame.

Our amplitude analysis is carried out in both the s -channel and the t -channel helicity frames for the $\pi^+ \pi^-$ dimeson system. The helicities of the initial and final nucleons are always defined in the s -channel helicity frame.

B. Observables

When the polarization of the recoil nucleon is not observed, the angular distribution $I(\theta, \varphi, \psi, \delta)$ of $\pi^+ \pi^-$ production on polarized nucleons at rest can be expressed in terms of the normalized distribution $W(\theta, \varphi, \psi, \delta)$:

$$I(\theta, \varphi, \psi, \delta) = W(\theta, \varphi, \psi, \delta) d^2\sigma / (dt dm), \quad (2.1)$$

where

$$\frac{d^2\sigma}{dt dm} = \int I(\theta, \varphi, \psi, \delta) d\Omega d\psi d(-\sin\delta) \quad (2.2)$$

is the $\pi^+ \pi^-$ production cross section at fixed values of s , t , and m . The distribution $W(\theta, \varphi, \psi, \delta)$ can be written as a sum of four terms:

$$W(\theta, \varphi, \psi, \delta) = W_0(\theta, \varphi) + P_T \cos \psi W_y(\theta, \varphi) + P_T \sin \psi W_x(\theta, \varphi) + P_L W_z(\theta, \varphi), \quad (2.3)$$

where $P_T = P \cos \delta$ and $P_L = P \sin \delta$ are the transverse and longitudinal components of target polarization \mathbf{P} with respect to the incident momentum in the reference frame of target nucleon at rest [29]. Only $W_0(\Omega)$ is measured in experiments on unpolarized targets. Parity conservation requires that W_0 and W_y (W_x and W_z) be symmetric (antisymmetric) in φ .

The $\pi^+\pi^-$ system is not produced, in general, in a state of definite spin, helicity, and parity. The polarization of the $\pi^+\pi^-$ system is described [16] by the spin-density matrix with complex matrix elements $\rho_{\lambda\lambda'}^{JJ'}$, where J, J' and λ, λ' are the meson spins and helicities, respectively. Omitting the indices J, J', λ, λ' for clarity, the SDM elements $\rho_{\lambda\lambda'}^{JJ'}$ for the $\pi^+\pi^-$ production on a polarized target have the general form [16,41–45]

$$4\pi W_0(\Omega) = (\rho_{ss} + \rho_{00} + 2\rho_{11}) + (\rho_{00} - \rho_{1-1})[3 \cos^2(\theta) - 1] - \rho_{1-1} 3 \sin^2(\theta) \cos(2\varphi) - \text{Re} \rho_{10} 3\sqrt{2} \sin(2\theta) \cos(\varphi) + \text{Re} \rho_{0s} 2\sqrt{3} \cos(\theta) - \text{Re} \rho_{1s} 2\sqrt{6} \sin(\theta) \cos(\varphi), \quad (2.6a)$$

$$4\pi W_y(\Omega) = (\rho_{ss}^y + \rho_{00}^y + 2\rho_{11}^y) + (\rho_{00}^y - \rho_{1-1}^y)[3 \cos^2(\theta) - 1] - \rho_{1-1}^y 3 \sin^2(\theta) \cos(2\varphi) - \text{Re} \rho_{10}^y 3\sqrt{2} \sin(2\theta) \cos(\varphi) + \text{Re} \rho_{0s}^y 2\sqrt{3} \cos(\theta) - \text{Re} \rho_{1s}^y 2\sqrt{6} \sin(\theta) \cos(\varphi), \quad (2.6b)$$

$$4\pi W_x(\Omega) = \text{Im} \rho_{1-1}^x 3 \sin^2(\theta) \sin(2\varphi) + \text{Im} \rho_{10}^x 3\sqrt{2} \sin(2\theta) \sin(\varphi) + \text{Im} \rho_{1s}^x 2\sqrt{6} \sin(2\theta) \sin(\varphi). \quad (2.6c)$$

In Eqs. (2.6), the indices JJ' were omitted and the helicity λ of $\pi^+\pi^-$ system is $\lambda = s$ and $\lambda = -1, 0, +1$ for the S wave and P wave, respectively. There are two linear relations among the matrix elements in (2.6):

$$\begin{aligned} \rho_{ss} + \rho_{00} + 2\rho_{11} &= 1, \\ \rho_{ss}^y + \rho_{00}^y + 2\rho_{11}^y &= A, \end{aligned} \quad (2.7)$$

where A is the polarized target asymmetry.

The unpolarized SDM elements (2.6a) were previously measured in experiments on unpolarized targets. The experiments using transversely polarized targets add polarized SDM elements (2.6b) and (2.6c) to SDM elements (2.6a) in a single measurement.

C. Amplitudes

The reaction $\pi^+n \rightarrow \pi^+\pi^-p$ is described by pion production amplitudes $H_{\lambda_p, 0\lambda_n}(s, t, m, \theta, \varphi)$, where λ_p and λ_n are the helicities of the proton and neutron, respectively. The production amplitudes can be expressed in terms of production amplitudes corresponding to definite meson spin J using an angular expansion

$$H_{\lambda_p, 0\lambda_n} = \sum_{J=0}^{\infty} \sum_{\lambda=-J}^{+J} (2J+1)^{1/2} H_{\lambda\lambda_p, 0\lambda_n}^J(s, t, m) d_{\lambda 0}^J(\theta) e^{i\lambda\varphi}, \quad (2.8)$$

where J is the spin and λ the helicity of the $(\pi^+\pi^-)$ meson system. The ‘‘partial-wave’’ amplitudes $H_{\lambda\lambda_p, 0\lambda_n}^J$ can be expressed in terms of nucleon helicity amplitudes

$$\rho = \rho^0 + P_T \cos \psi \rho^y + P_T \sin \psi \rho^x + P_L \rho^z. \quad (2.4)$$

The components of angular distribution, $W_k(\theta, \psi)$, $k=0, y, x, z$, can be expressed in terms of the matrix elements of the corresponding component ρ^k of the SDM elements [16]

$$W_k(\Omega) = \sum_{J, \lambda} \sum_{J', \lambda'} \rho_{\lambda\lambda'}^{k, JJ'} Y_{\lambda}^J(\Omega) Y_{\lambda'}^{J'*}(\Omega), \quad (2.5)$$

where $Y_{\lambda}^J(\Omega)$ are spherical harmonics. It is understood that in (2.5) there are real parts $\text{Re} \rho^k$ and imaginary parts $\text{Im} \rho^k$ of SDM elements for $k=0, y$ and $k=x, z$, respectively.

The Saclay experiment did not measure $W_z(\Omega)$ since the longitudinal component of polarization $P_L=0$. Assuming S - and P -wave dominance, the explicit form of the π^+ angular distributions in terms of the $\pi^+\pi^-$ SDM elements at fixed values of s, t, m reads as

with definite t -channel exchange naturality. The nucleon s -channel helicity amplitudes describing the production of the $(\pi^+\pi^-)$ system in the S - and P -wave states are

$$\begin{aligned} 0^{-\frac{1}{2}+} \rightarrow 0^{+\frac{1}{2}+}: & H_{0+,0+}^0 = S_0, \\ & H_{0+,0-}^0 = S_1, \end{aligned} \quad (2.9a)$$

$$\begin{aligned} 0^{-\frac{1}{2}+} \rightarrow 1^{-\frac{1}{2}+}: & H_{0+,0+}^1 = L_0, \\ & H_{0+,0-}^1 = L_1, \end{aligned} \quad (2.9b)$$

$$H_{\pm 1+,0+}^1 = \frac{N_0 \pm U_0}{\sqrt{2}},$$

$$H_{\pm 1+,0-}^1 = \frac{N_1 \pm U_1}{\sqrt{2}}.$$

At large s , the amplitudes N_0 and N_1 are both dominated by natural A_2 exchange. The amplitudes S_n, L_n, U_n , $n=0, 1$ are dominated by unnatural exchanges: A_1 exchange for $n=0$ and π exchange for $n=1$. The index $n = |\lambda_n - \lambda_p|$ is nucleon helicity flip.

The observables obtained in experiments on a transversely polarized nucleon target in which recoil nucleon polarization is not observed are most simply related to nucleon transversity amplitudes (NTA) of definite naturality. In general, in a reaction $1+2 \rightarrow 3+4$, mixed helicity-transversity amplitudes $T_{\lambda_3\tau_4, \lambda_1\tau_2}^J$ are defined in terms of helicity amplitudes $H_{\lambda_3\lambda_4, \lambda_1\lambda_2}^J$ as

$$T_{\lambda_3\tau_4, \lambda_1\tau_2}^J = \sum_{\lambda_2, \lambda_4} \mathcal{D}_{\tau_4\lambda_4}^{(S_4)*} \mathcal{D}_{\tau_2\lambda_2}^{(S_2)} H_{\lambda_3\lambda_4, \lambda_1\lambda_2}^J, \quad (2.10)$$

where $\mathcal{D}_{\lambda\tau}^{(S)}$ are rotation matrices describing the transversity frame first defined by Kotanski [46,47] (see also the Appendix of Ref. [31]). We note that the use of transversity in the study of ρ production goes back many years [48] and that hybrid amplitudes mixing helicity and transversity were also used in the analyses of pion photoproduction [49].

For S - and P -wave amplitudes in the reaction $\pi^+ n \rightarrow \pi^+ \pi^- p$, we define the following NTA of definite naturality:

$$S = \frac{1}{\sqrt{2}}(S_0 + iS_1) = -\frac{i}{\sqrt{2}}T_{0\uparrow,0\downarrow}^{(0)}, \quad (2.11a)$$

$$\bar{S} = \frac{1}{\sqrt{2}}(S_0 - iS_1) = +\frac{i}{\sqrt{2}}T_{0\downarrow,0\uparrow}^{(0)},$$

$$L = \frac{1}{\sqrt{2}}(L_0 + iL_1) = -\frac{i}{\sqrt{2}}T_{0\uparrow,0\downarrow}^{(1)}, \quad (2.11b)$$

$$\bar{L} = \frac{1}{\sqrt{2}}(L_0 - iL_1) = +\frac{i}{\sqrt{2}}T_{0\downarrow,0\uparrow}^{(1)},$$

$$U = \frac{1}{\sqrt{2}}(U_0 + iU_1) = -iT_{+1\uparrow,0\downarrow}^{(1)} = +iT_{-1\uparrow,0\downarrow}^{(1)}, \quad (2.11c)$$

$$\bar{U} = \frac{1}{\sqrt{2}}(U_0 - iU_1) = +iT_{+1\downarrow,0\uparrow}^{(1)} = -iT_{-1\downarrow,0\uparrow}^{(1)},$$

$$N = \frac{1}{\sqrt{2}}(N_0 - iN_1) = T_{+1\downarrow,0\downarrow}^{(1)} = T_{-1\downarrow,0\downarrow}^{(1)}, \quad (2.11d)$$

$$\bar{N} = \frac{1}{\sqrt{2}}(N_0 + iN_1) = T_{+1\uparrow,0\uparrow}^{(1)} = T_{-1\uparrow,0\uparrow}^{(1)}.$$

The symbols \uparrow and \downarrow in Eqs. (2.11) denote the nucleon transversities parallel (or ‘‘up’’) and antiparallel (or ‘‘down’’) to the normal \mathbf{n} of the production plane, respectively. The following table summarizes the transversity states of target neutrons and recoil protons, and the dimeson helicity is corresponding to the amplitudes (2.11):

	n	p	$(\pi^+ \pi^-)$
S, L	\uparrow	\downarrow	0
\bar{S}, \bar{L}	\downarrow	\uparrow	0
U	\uparrow	\downarrow	+1 or -1
\bar{U}	\downarrow	\uparrow	+1 or -1
N	\downarrow	\downarrow	+1 or -1
\bar{N}	\uparrow	\uparrow	+1 or -1

(2.12)

Table (2.12) shows that the transversity amplitudes S, L, U, N ($\bar{S}, \bar{L}, \bar{U}, \bar{N}$) describe the production of the dimeson state with the recoil nucleon transversity down (up) relative to the production plane. The amplitudes $S, \bar{S}, L, \bar{L}, U, \bar{U}$ correspond to nucleon transversity flip while N and \bar{N} are nucleon transversity nonflip amplitudes.

In (2.11) we assumed P -parity conservation. Parity conservation requires that, in the transversity frame, the dimeson production with helicities $\lambda = \pm 1$ depends only on the transversities of the initial and final nucleons. The

amplitudes U, \bar{U}, N, \bar{N} do not distinguish between the dimeson helicity states with $\lambda = +1$ or -1 . Also, dimeson production with helicity $\lambda = 0$ is forbidden by parity conservation when the initial and final nucleons have the same transversities.

D. Observables in terms of normalized amplitudes

The spin-density-matrix elements $\rho_{\lambda\lambda'}^{k, JJ'}$ [Eq. (2.4)] are defined in terms of amplitudes (2.8) as follows [16]:

$$\rho_{\lambda\lambda'}^{k, JJ'} \Sigma = \frac{1}{2} \sum_{\lambda_p} \sum_{\lambda_n \lambda'_n} H_{\lambda\lambda_p, 0\lambda_n}^J \sigma^k_{\lambda_n \lambda'_n} H_{\lambda'\lambda_p, 0\lambda'_n}^{J'*}, \quad (2.13)$$

where $\sigma^0 \equiv 1$ and $\sigma^k, k = x, y, z$ are the Pauli matrices. In our normalization, the integrated cross section $\Sigma \equiv d^2\sigma/dm dt$ is given by

$$\begin{aligned} \Sigma &= \sum_{n=0,1} |S_n|^2 + |L_n|^2 + |U_n|^2 + |N_n|^2 \\ &= |S|^2 + |\bar{S}|^2 + |L|^2 + |\bar{L}|^2 \\ &\quad + |U|^2 + |\bar{U}|^2 + |N|^2 + |\bar{N}|^2. \end{aligned} \quad (2.14)$$

In the Saclay experiment the cross section has not been measured. Consequently, we will work with normalized amplitudes corresponding to

$$\Sigma = \frac{d^2\sigma}{dm dt} \equiv 1. \quad (2.15)$$

Using (2.13) and (2.15), the relations for SDM elements in terms of normalized helicity amplitudes read as follows.

Unpolarized SDM elements:

$$\begin{aligned} \rho_{ss} + \rho_{00} + 2\rho_{11} &= \sum_{n=0,1} |S_n|^2 + |L_n|^2 + |U_n|^2 + |N_n|^2, \\ \rho_{00} + \rho_{11} &= \sum_{n=0,1} |L_n|^2 - \frac{1}{2}(|N_n|^2 + |U_n|^2), \\ \rho_{1-1} &= \sum_{n=0,1} \frac{1}{2}(|N_n|^2 - |U_n|^2), \\ \sqrt{2} \operatorname{Re}\rho_{10} &= \sum_{n=0,1} \operatorname{Re}(U_n L_n^*), \end{aligned} \quad (2.16a)$$

$$\sqrt{2} \operatorname{Re}\rho_{1s} = \sum_{n=0,1} \operatorname{Re}(U_n S_n^*),$$

$$\operatorname{Re}\rho_{0s} = \sum_{n=0,1} \operatorname{Re}(L_n S_n^*).$$

Polarized SDM elements:

$$\begin{aligned} \rho_{ss}^y + \rho_{00}^y + 2\rho_{11}^y &= 2 \operatorname{Im}(S_0 S_1^* + L_0 L_1^* + U_0 U_1^* + N_0 N_1^*), \\ \rho_{00}^y - \rho_{11}^y &= \operatorname{Im}(2L_0 L_1^* - N_0 N_1^* - U_0 U_1^*), \\ \rho_{1-1}^y &= \operatorname{Im}(N_0 N_1^* - U_0 U_1^*), \end{aligned} \quad (2.16b)$$

$$\sqrt{2} \operatorname{Re}\rho_{10}^y = \operatorname{Im}(U_0 L_1^* - U_1 L_0^*),$$

$$\sqrt{2} \operatorname{Re}\rho_{1s}^y = \operatorname{Im}(U_0 S_1^* - U_1 S_0^*),$$

$$\operatorname{Re}\rho_{0s}^y = \operatorname{Im}(L_0 S_1^* - L_1 S_0^*),$$

$$-\operatorname{Im}\rho_{1-1}^x = \operatorname{Im}(N_0 U_1^* + N_1 U_0^*),$$

$$\sqrt{2} \operatorname{Im}\rho_{10}^x = \operatorname{Im}(N_0 L_1^* + N_1 L_0^*), \quad (2.16c)$$

$$\sqrt{2} \operatorname{Im}\rho_{1s}^x = \operatorname{Im}(N_0 S_1^* + N_1 S_0^*).$$

Only the polarization-dependent SDM elements measure the nucleon helicity flip-nonflip interference. The observables (2.16b) and (2.16c) measure the interference between the amplitudes of the same and opposite naturalities, respectively.

To express the observables in terms of normalized nucleon transversity amplitudes (2.11), we first introduce partial-wave cross sections $\sigma(A)$ and partial-wave polarizations $\tau(A)$ defined for amplitudes $A=S, L, U, N$ as

$$\begin{aligned}\sigma(A) &= |A_0|^2 + |A_1|^2 = |A|^2 + |\bar{A}|^2, \\ \tau(A) &= 2\epsilon \operatorname{Im}(A_0 A_1^*) = |A|^2 - |\bar{A}|^2,\end{aligned}\quad (2.17)$$

where $\epsilon = +1$ for $A=S, L, U$ and $\epsilon = -1$ for $A=N$. In our normalization the reaction cross section is

$$\Sigma = \sigma(S) + \sigma(L) + \sigma(U) + \sigma(N) = 1. \quad (2.18)$$

Then the relations for SDM elements (2.16a) and (2.16b) in terms of normalized nucleon transversity amplitudes (2.11) and quantities (2.17) read

$$\begin{aligned}\rho_{ss} + \rho_{00} + 2\rho_{11} &= \sigma(S) + \sigma(L) + \sigma(U) + \sigma(N), \\ \rho_{00} - \rho_{11} &= \sigma(L) - \frac{1}{2}[\sigma(U) + \sigma(N)],\end{aligned}\quad (2.19a)$$

$$\begin{aligned}\rho_{1-1} &= -\frac{1}{2}[\sigma(U) - \sigma(N)], \\ \rho_{ss}^y + \rho_{00}^y + 2\rho_{11}^y &= \tau(S) + \tau(L) + \tau(U) - \tau(N), \\ \rho_{00}^y - \rho_{11}^y &= \tau(L) - \frac{1}{2}[\tau(U) - \tau(N)],\end{aligned}\quad (2.19b)$$

$$\begin{aligned}\rho_{1-1}^y &= -\frac{1}{2}[\tau(U) + \tau(N)], \\ \sqrt{2} \operatorname{Re} \rho_{10} &= \operatorname{Re}(UL^* + \bar{U}\bar{L}^*), \\ \sqrt{2} \operatorname{Re} \rho_{1s} &= \operatorname{Re}(US^* + \bar{U}\bar{S}^*),\end{aligned}\quad (2.20a)$$

$$\begin{aligned}\operatorname{Re} \rho_{0s} &= \operatorname{Re}(LS^* + \bar{L}\bar{S}^*), \\ \sqrt{2} \operatorname{Re} \rho_{10}^y &= \operatorname{Re}(UL^* - \bar{U}\bar{L}^*), \\ \sqrt{2} \operatorname{Re} \rho_{1s}^y &= \operatorname{Re}(US^* - \bar{U}\bar{S}^*),\end{aligned}\quad (2.20b)$$

$$\operatorname{Re} \rho_{0s}^y = \operatorname{Re}(LS^* - \bar{L}\bar{S}^*).$$

The relations (2.19) and (2.20) suggest the introduction of new observables which are the sum and difference of the SDM elements (2.16a) and (2.16b). Using the notation of (2.7), the first group of new observables reads

$$\begin{aligned}a_1 &= \frac{1}{2}(1+A) = |S|^2 + |L|^2 + |U|^2 + |\bar{N}|^2, \\ a_2 &= [(\rho_{00} - \rho_{11}) + (\rho_{00}^y - \rho_{11}^y)] \\ &= 2|L|^2 - |U|^2 - |\bar{N}|^2, \\ a_3 &= [\rho_{1-1} + \rho_{1-1}^y] = |\bar{N}|^2 - |U|^2, \\ a_4 &= \frac{1}{\sqrt{2}}[\operatorname{Re} \rho_{10} + \operatorname{Re} \rho_{10}^y] = |U||L|\cos(\gamma_{UL}), \\ a_5 &= \frac{1}{\sqrt{2}}[\operatorname{Re} \rho_{1s} + \operatorname{Re} \rho_{1s}^y] = |U||S|\cos(\gamma_{US}), \\ a_6 &= \frac{1}{2}[\operatorname{Re} \rho_{0s} + \operatorname{Re} \rho_{0s}^y] = |L||S|\cos(\gamma_{LS}).\end{aligned}\quad (2.21a)$$

Similar equations relate the difference of SDM elements to amplitudes of opposite transversity. The second group of observables is defined as

$$\begin{aligned}\bar{a}_1 &= \frac{1}{2}[1-A] = |\bar{S}|^2 + |\bar{L}|^2 + |\bar{U}|^2 + |N|^2, \\ \bar{a}_2 &= [(\rho_{00} - \rho_{11}) - (\rho_{00}^y - \rho_{11}^y)] \\ &= 2|\bar{L}|^2 - |\bar{U}|^2 - |N|^2,\end{aligned}\quad (2.22a)$$

$$\begin{aligned}\bar{a}_3 &= [\rho_{1-1} - \rho_{1-1}^y] = |N|^2 - |\bar{U}|^2, \\ \bar{a}_4 &= \frac{1}{\sqrt{2}}[\operatorname{Re} \rho_{10} - \operatorname{Re} \rho_{10}^y] = |\bar{U}||\bar{L}|\cos(\bar{\gamma}_{UL}), \\ \bar{a}_5 &= \frac{1}{\sqrt{2}}[\operatorname{Re} \rho_{1s} - \operatorname{Re} \rho_{1s}^y] = |\bar{U}||\bar{S}|\cos(\bar{\gamma}_{US}), \\ \bar{a}_6 &= \frac{1}{2}[\operatorname{Re} \rho_{0s} - \operatorname{Re} \rho_{0s}^y] = |\bar{L}||\bar{S}|\cos(\bar{\gamma}_{LS}).\end{aligned}\quad (2.22b)$$

In Eqs. (2.21b) and (2.22b), we have introduced explicitly the cosines of relative phases between the nucleon transversity amplitudes.

The SDM elements (2.16c) form the third group of observables. In terms of normalized nucleon transversity amplitudes, we have

$$\begin{aligned}b_1 &= -\operatorname{Im} \rho_{1-1}^x = \operatorname{Re}(NU^* - \bar{N}\bar{U}^*), \\ b_2 &= \sqrt{2} \operatorname{Im} \rho_{10}^x = \operatorname{Re}(NL^* - \bar{N}\bar{L}^*), \\ b_3 &= \sqrt{2} \operatorname{Im} \rho_{1s}^x = \operatorname{Re}(NS^* - \bar{N}\bar{S}^*).\end{aligned}\quad (2.23)$$

While the observables $a_i, \bar{a}_i, i=1, 2, \dots, 6$ are determined by the transverse-polarization component $P_T \cos\psi$ perpendicular to the scattering plane, the observables in (2.23) are determined by the transverse-polarization component $P_T \sin\psi$ in the scattering plane. In the Saclay experiment, $P_T \sin\psi$ was small and b_1, b_2, b_3 were thus measured with a lesser precision than the observables (2.21) and (2.22).

Relations for observables in terms of unnormalized amplitudes can be obtained by multiplying the left-hand sides of (2.16)–(2.23) by the measured reaction cross section Σ . The unnormalized amplitudes have the same relative phases as the normalized amplitudes, but their moduli are given by $|A_0|^2 \Sigma, |A_1|^2 \Sigma$ or by $|A|^2 \Sigma, |\bar{A}|^2 \Sigma$ for $A=S, L, U, N$. In this paper we will work only with normalized amplitudes.

III. THE METHOD OF ANALYSIS

The observables measured in $\pi^+n_{\uparrow} \rightarrow \pi^+\pi^-p$ on a transversely polarized target organize themselves into three distinct groups (2.21), (2.22), and (2.23) in the kinematical region of (m, t) where only the S and P waves dominate. The first group (2.21) involves four moduli $|S|^2, |L|^2, |U|^2$, and $|\bar{N}|^2$ and three cosines of relative phases $\cos(\gamma_{SL}), \cos(\gamma_{SU}),$ and $\cos(\gamma_{LU})$. The second group (2.22) involves the same amplitudes but with opposite nucleon transversities. The third group (2.23) adds two new phases relative to the only two natural exchange amplitudes involved, N and \bar{N} . It is convenient to choose γ_{NS} and $\bar{\gamma}_{NS}$ because they are helicity frame invariant.

The relative phase between the two groups of amplitudes of opposite nucleon transversities does not enter at all into the measured observables (2.21), (2.22), and (2.23), and it is therefore unknown. Its determination requires measurements of recoil nucleon polarization.

Our task is to express amplitudes in terms of observables. In the following sections we do this for the four moduli and the three cosines in Eqs. (2.21) and (2.22). The analytical solution has a twofold ambiguity. We discuss some of its properties and limitations on its experimental determination.

Equations (2.23) are solved for sines and cosines of relative phases γ_{NS} and $\bar{\gamma}_{NS}$ in the Appendix. The obtained analytical solution has a 32-fold ambiguity. Because of this fact and because the input data b_1, b_2, b_3 have large errors in the Saclay experiment, we have not calculated these relative phases in our amplitude analysis.

A. The system of equations

Equations (2.19a) can be solved for three mixed normalized partial-wave cross sections:

$$\begin{aligned} \sigma(L) + \frac{1}{3}\sigma(S) &= \frac{1}{3}[1 + 2(\rho_{00} + \rho_{11})], \\ \sigma(U) + \frac{1}{3}\sigma(S) &= \frac{1}{3}[1 - (\rho_{00} - \rho_{11})] - \rho_{1-1}, \\ \sigma(N) + \frac{2}{3}\sigma(S) &= \frac{1}{3}[1 - (\rho_{00} - \rho_{11})] + \rho_{1-1}. \end{aligned} \quad (3.1a)$$

With the notation of (2.7), we similarly get from (2.19b) three mixed partial-wave polarizations:

$$\begin{aligned} \tau(L) + \frac{1}{3}\tau(S) &= \frac{1}{3}[A + 2(\rho_{00}^y - \rho_{11}^y)], \\ \tau(U) + \frac{1}{3}\tau(S) &= \frac{1}{3}[A - (\rho_{00}^y - \rho_{11}^y)] - \rho_{1-1}^y, \\ -\tau(N) + \frac{1}{3}\tau(S) &= \frac{1}{3}[A - (\rho_{00}^y - \rho_{11}^y)] + \rho_{1-1}^y. \end{aligned} \quad (3.1b)$$

Using the notation of (2.21) and (2.22) for sums and differences of SDM elements, we can calculate from (3.1) the following combinations of moduli squared:

$$\begin{aligned} |L|^2 + \frac{1}{3}|S|^2 &= \frac{1}{3}(a_1 + a_2), \\ |U|^2 + \frac{1}{3}|S|^2 &= \frac{1}{6}(2a_1 - a_2 - 3a_3), \\ |\bar{N}|^2 + \frac{1}{3}|S|^2 &= \frac{1}{6}(2a_1 - a_2 + 3a_3), \\ |\bar{L}|^2 + \frac{1}{3}|\bar{S}|^2 &= \frac{1}{3}(\bar{a}_1 + \bar{a}_2), \\ |\bar{U}|^2 + \frac{1}{3}|\bar{S}|^2 &= \frac{1}{6}(2\bar{a}_1 - \bar{a}_2 - 3\bar{a}_3), \\ |N|^2 + \frac{1}{3}|\bar{S}|^2 &= \frac{1}{6}(2\bar{a}_1 - \bar{a}_2 + 3\bar{a}_3). \end{aligned} \quad (3.2a)$$

$$\begin{aligned} |\bar{L}|^2 + \frac{1}{3}|\bar{S}|^2 &= \frac{1}{3}(\bar{a}_1 + \bar{a}_2), \\ |\bar{U}|^2 + \frac{1}{3}|\bar{S}|^2 &= \frac{1}{6}(2\bar{a}_1 - \bar{a}_2 - 3\bar{a}_3), \\ |N|^2 + \frac{1}{3}|\bar{S}|^2 &= \frac{1}{6}(2\bar{a}_1 - \bar{a}_2 + 3\bar{a}_3). \end{aligned} \quad (3.2b)$$

From (2.21b) and (2.22b) we get cosines in terms of three moduli

$$\cos(\gamma_{UL}) = \frac{a_4}{|U||L|}, \quad (3.3a)$$

$$\begin{aligned} \cos(\gamma_{US}) &= \frac{a_5}{|U||S|}, \quad \cos(\gamma_{LS}) = \frac{a_6}{|L||S|}, \\ \cos(\bar{\gamma}_{UL}) &= \frac{\bar{a}_4}{|\bar{U}||\bar{L}|}, \\ \cos(\bar{\gamma}_{US}) &= \frac{\bar{a}_5}{|\bar{U}||\bar{S}|}, \quad \cos(\bar{\gamma}_{LS}) = \frac{\bar{a}_6}{|\bar{L}||\bar{S}|}. \end{aligned} \quad (3.3b)$$

The relations (3.2a), (3.3a) and (3.2b), (3.3b) provide two sets of six equations, each for four moduli and three cosines of amplitudes of opposite nucleon transversities.

Evidently, each set requires one additional equation for its moduli.

The additional equations are provided by the relative phases which are not independent:

$$\begin{aligned} \gamma_{UL} - \gamma_{US} + \gamma_{LS} &= (\phi_U - \phi_L) - (\phi_U - \phi_S) \\ &+ (\phi_L - \phi_S) = 0, \\ \bar{\gamma}_{UL} - \bar{\gamma}_{US} + \bar{\gamma}_{LS} &= (\bar{\phi}_U - \bar{\phi}_L) - (\bar{\phi}_U - \bar{\phi}_S) \\ &+ (\bar{\phi}_L - \bar{\phi}_S) = 0. \end{aligned} \quad (3.4)$$

These conditions lead to nonlinear relations between the cosines:

$$\begin{aligned} \cos^2(\gamma_{UL}) + \cos^2(\gamma_{US}) + \cos^2(\gamma_{LS}) \\ - 2\cos\gamma_{UL}\cos\gamma_{US}\cos\gamma_{LS} &= 1, \\ \cos^2(\bar{\gamma}_{UL}) + \cos^2(\bar{\gamma}_{US}) + \cos^2(\bar{\gamma}_{LS}) \\ - 2\cos\bar{\gamma}_{UL}\cos\bar{\gamma}_{US}\cos\bar{\gamma}_{LS} &= 1. \end{aligned} \quad (3.5)$$

Similar relations also hold for the sines. Substituting from (3.3) into (3.5) gives

$$a_4^2|S|^2 + a_5^2|L|^2 + a_6^2|U|^2 - |S|^2|L|^2|U|^2 = 2a_4a_5a_6, \quad (3.6a)$$

$$\bar{a}_4^2|\bar{S}|^2 + \bar{a}_5^2|\bar{L}|^2 + \bar{a}_6^2|\bar{U}|^2 - |\bar{S}|^2|\bar{L}|^2|\bar{U}|^2 = 2\bar{a}_4\bar{a}_5\bar{a}_6. \quad (3.6b)$$

The two sets of equations (3.2a), (3.6a), and (3.2b), (3.6b) are now both complete and solvable for the moduli. The known moduli then determine cosines from (3.3a) and (3.3b).

B. Analytical solution for moduli

We first use the relations (3.2a) to obtain

$$\begin{aligned} |S|^2 &= (a_1 + a_2) - 3|L|^2, \\ |U|^2 &= |L|^2 - \frac{1}{2}(a_2 + a_3), \\ |\bar{N}|^2 &= |L|^2 - \frac{1}{2}(a_2 - a_3). \end{aligned} \quad (3.7)$$

Substituting (3.7) into (3.6a) we get a cubic equation for $|L|^2 \equiv x$:

$$ax^3 + bx^2 + cx + d = 0, \quad (3.8)$$

where

$$\begin{aligned} a &= 3, \\ b &= -3[\frac{1}{3}(a_1 + a_2) + \frac{1}{2}(a_2 + a_3)], \\ c &= \frac{1}{2}(a_1 + a_2)(a_2 + a_3) - 3a_4^2 + a_5^2 + a_6^2, \\ d &= (a_1 + a_2)a_4^2 - \frac{1}{2}(a_2 + a_3)a_6^2 - 2a_4a_5a_6. \end{aligned}$$

To solve (3.8) we write

$$x = y - y_0 \quad (3.9)$$

and require that (3.8) transforms to a form

$$y^3 + 3Py + 2Q = 0. \quad (3.10) \quad \text{tween the two solutions}$$

This is accomplished with

$$y_0 = \frac{b}{3a},$$

$$P = - \left[\frac{b}{3a} \right]^2 + \left[\frac{c}{3a} \right], \quad (3.11)$$

$$2Q = - \left[\frac{b}{3a} \right] \left[2P + \frac{c}{3a} \right] + \frac{d}{a}.$$

We now define

$$R = \text{sgn}(Q) \sqrt{|P|},$$

$$V = \frac{Q}{R^3} \geq 0. \quad (3.12)$$

There are three categories of solutions [50] of cubic equations (3.10) and (3.8). They are given in the Table I.

In most (m, t) bins in the kinematic regions (1.3) and (1.4) we found $R > 0$ and negative values for the third solution $x_3 = r_3 - y_0$, irrespective of which category of solution the mean values of input data yield in a given (m, t) bin. This negative solution for $x = |L|^2$ is rejected.

The three solutions of cubic equation (3.8) are all real only when $P < 0$ and $Q^2 + P^3 \leq 0$. The two solutions of interest,

$$x_1 = R \cos \left[\frac{\phi}{3} \right] + \sqrt{3} R \sin \left[\frac{\phi}{3} \right] - y_0,$$

$$x_2 = R \cos \left[\frac{\phi}{3} \right] - \sqrt{3} R \sin \left[\frac{\phi}{3} \right] - y_0, \quad (3.13)$$

are always ordered

$$x_1 \geq x_2 \quad (3.14)$$

for positive R . In our kinematic region both solutions are generally positive and close.

For real solutions (3.13) we have $0 \leq \cos \phi \leq 1$. The two solutions are close when ϕ is small. Then the distance be-

$$\Delta x = x_1 - x_2 = 2\sqrt{3} R \sin \left[\frac{\phi}{3} \right] \quad (3.15)$$

is also small and positive. The two solutions are equal when $\phi = 0$, i.e., when

$$Q^2 = |P|^3. \quad (3.16)$$

This case has not occurred for the mean values of input data in the kinematic regions (1.3) and (1.4). We therefore treat both solutions (3.13) as distinct.

The two solutions (3.13) for $|L|^2$ lead to two solutions for the moduli (3.7) and the cosines, (3.3a). The system of equations (3.2b), (3.6b), and (3.3b) for four moduli and three cosines of opposite transversities is solved similarly. As a result, there are two pairs of solutions for each group of transversity amplitudes which we label in accordance with (3.14) as solutions 1 and 2.

C. Physical solution

The physical solutions of cubic equation (3.8) for $|L|^2$ must be real and positive, but that is not the only requirement. The solution for $|L|^2$ also must be normalized,

$$0 \leq |L|^2 \leq 1, \quad (3.17a)$$

and it must produce physical solutions for the moduli (3.7) and the cosines (3.3a):

$$0 \leq |A|^2 \leq 1, \quad A = S, U, \bar{N}, \quad (3.17b)$$

$$0 \leq (\cos \gamma_k)^2 \leq 1, \quad k = UL, US, LS. \quad (3.17c)$$

There are similar constraints on the solutions for $|\bar{L}|^2$ in the second group.

We will show elsewhere [51] how Eqs. (3.2a) and (3.3a) transform the conditions (3.17) into stricter inequalities. The physical solutions for $|L|^2$ and $|\bar{L}|^2$ are then confined to certain intervals within the closed interval $[0, 1]$:

$$0 \leq x_{\min} \leq |L|^2 \leq x_{\max} \leq 1, \quad (3.18)$$

$$0 \leq \bar{x}_{\min} \leq |\bar{L}|^2 \leq \bar{x}_{\max} \leq 1.$$

TABLE I. Three categories of solutions of Eq. (3.10).

$P < 0$ $Q^2 + P^3 \leq 0$ $V = \cos(\phi)$	$P < 0$ $Q^2 + P^3 > 0$ $V = \cosh(\phi)$	$P > 0$ $V = \sinh(\phi)$
$r_1 = +2R \cos \left[\frac{\pi - \phi}{3} \right]$	$c_1 = R \cosh \left[\frac{\phi}{3} \right] + i\sqrt{3} R \sinh \left[\frac{\phi}{3} \right]$	$c_2 = R \sinh \left[\frac{\phi}{3} \right] + i\sqrt{3} R \cosh \left[\frac{\phi}{3} \right]$
$r_2 = +2R \cos \left[\frac{\pi + \phi}{3} \right]$	c_1^*	c_2^*
$r_3 = -2R \cos \left[\frac{\phi}{3} \right]$	$r_3' = -2R \cosh \left[\frac{\phi}{3} \right]$	$r_3'' = -2R \sinh \left[\frac{\phi}{3} \right]$

Originating in the requirement of self-consistency of physical conditions (3.17) with the system of equations (3.2a) and (3.3a), the new bounds imply five linear and one nonlinear independent inequality constraints on the observables a_i , $i = 1, \dots, 6$. The constraints read [51]

$$\begin{aligned} \frac{1}{3}(a_1 + a_2) &\leq 1, \\ \frac{1}{2}(a_2 + a_3) &\leq 1, \\ \frac{1}{2}|a_3| &\leq \frac{1}{3}(a_1 + a_2) - \frac{1}{2}a_2, \\ \frac{1}{2}|a_3| &\leq 1 - [\frac{1}{3}(a_1 + a_2) - \frac{1}{2}a_2], \\ \frac{1}{2}|a_4| &\leq \sqrt{1 - \frac{1}{2}(a_2 + a_3)}, \\ \frac{2}{\sqrt{3}}|a_5| &\leq \frac{1}{3}(a_1 + a_2) - \frac{1}{2}(a_2 + a_3), \\ \frac{2}{\sqrt{3}}|a_6| &\leq \frac{1}{3}(a_1 + a_2). \end{aligned} \quad (3.19)$$

Similar constraints hold for the observables \bar{a}_i , $i = 1, \dots, 6$.

Additional constraints on the solutions of the cubic equation (3.8) come from the requirement of positivity of spin-density matrix and from Schwartz inequalities for certain unpolarized SDM elements. Neither requirement imposes new conditions on $|L|^2$ and $|\bar{L}|^2$ separately, but rather on their sum [51], i.e., on a partial-wave cross section $\sigma(L) = |L|^2 + |\bar{L}|^2$. Combining Schwartz inequalities with (2.7) from the assumption S - and P -wave dominance leads to conditions

$$\sigma(L)_{\min} \leq |L|^2 + |\bar{L}|^2 \leq \sigma(L)_{\max}, \quad (3.20)$$

while higher-rank positivity conditions lead to nonlinear relations between partial-wave cross sections [51,52]. The significance of these constraints is in coupling the selection of solutions for $|L|^2$ with the selection of solutions for $|\bar{L}|^2$ [which in (3.18) were made independently]. These constraints also lead to nonlinear conditions on SDM elements.

The requirement that the solutions of (3.8) be all real for $Q > 0$ imposes additional nonlinear constraints

$$\begin{aligned} P < 0, \quad Q^2 + P^3 &\leq 0, \\ \bar{P} < 0, \quad \bar{Q}^2 + \bar{P}^3 &\leq 0. \end{aligned} \quad (3.21)$$

In principle, all constraints on SDM elements from (3.19), Schwartz inequalities, positivity, and reality (3.21) should be imposed during experimental data analysis on the maximum-likelihood function. This requires use of methods for constrained optimization [53,54] and special programs such as MINOS 5.0, developed recently at Stanford University [55]. Imposing nonlinear constraints requires bins of small size, and thus experiments with very high statistics.

D. Nucleon helicity amplitudes

Before we present and discuss our results, we shall note several relations between the moduli of nucleon transversity amplitudes $|A|^2$ and $|\bar{A}|^2$, and the moduli of nucleon helicity amplitudes $|A_0|^2$ and $|A_1|^2$, which will be useful

for their physical interpretation.

From (2.11) we obtain

$$\begin{aligned} 2|A|^2 &= |A_0|^2 + |A_1|^2 + 2\epsilon|A_0||A_1|\sin(\phi_0 - \phi_1), \\ 2|\bar{A}|^2 &= |A_0|^2 + |A_1|^2 - 2\epsilon|A_0||A_1|\sin(\phi_0 - \phi_1), \end{aligned} \quad (3.22)$$

where $\epsilon = +1$ for $A = S, L, U$ and $\epsilon = -1$ for $A = N$. ϕ_0 and ϕ_1 are phases of helicity amplitudes A_0 and A_1 , respectively. It follows from (3.22) that when

$$|A| \neq |\bar{A}| \quad \text{then} \quad |A_0| \neq 0, \quad |A_1| \neq 0, \quad \text{and} \quad \phi_0 - \phi_1 \neq 0. \quad (3.23)$$

In particular, when one of the moduli of transversity amplitudes A and \bar{A} is zero or small, the modulus of the amplitude with opposite transversity attains its maximum or near maximum value. When

$$|A| = |\bar{A}| \quad \text{then either} \quad |A_0| \quad \text{or} \quad |A_1| = 0 \quad (\text{but not both}), \quad \text{or} \quad \phi_0 - \phi_1 = 0. \quad (3.24)$$

Note that $|A_0| = |A_1| = 0$ only when $|A| = |\bar{A}| = 0$. The partial-wave polarization defined in (2.17),

$$\tau(A) = |A|^2 - |\bar{A}|^2 = 2\epsilon|A_0||A_1|\sin(\phi_0 - \phi_1), \quad (3.25)$$

determines the sign of relative phase $\phi_0 - \phi_1$. A crossover of moduli $|A|$ and $|\bar{A}|$ of transversity amplitudes gives rise to a change of sign in τ and in the relative phase of corresponding helicity amplitudes. The ambiguity in (3.24) cannot be resolved when the polarization τ has a zero without change of sign (a double zero).

The inverse relations read

$$\begin{aligned} 2|A_0|^2 &= |A|^2 + |\bar{A}|^2 + 2\epsilon|A||\bar{A}|\cos(\phi - \bar{\phi}), \\ 2|A_1|^2 &= |A|^2 + |\bar{A}|^2 - 2\epsilon|A||\bar{A}|\cos(\phi - \bar{\phi}), \end{aligned} \quad (3.26)$$

where ϕ and $\bar{\phi}$ are the phases of transversity amplitudes A and \bar{A} , respectively. From (3.26) we get

$$\omega(A) = |A_0|^2 - |A_1|^2 = 2\epsilon|A||\bar{A}|\cos(\phi - \bar{\phi}). \quad (3.27)$$

The relative magnitude of moduli $|A_0|$ and $|A_1|$ of helicity amplitudes is thus related to the relative phase $\phi - \bar{\phi}$ between the transversity amplitudes with recoil nucleon spin ‘‘down’’ and ‘‘up.’’ The relative phases $\bar{\phi} - \phi$ are not determined in experiments using only transversely polarized targets. It follows from the inverse relations (3.26) that the moduli $|A_0|$ and $|A_1|$ of helicity amplitudes are unknown, and, in general, $|A_0| \neq |A_1|$. However, the relations (3.26) imply that, when

$$|A| \quad \text{or} \quad |\bar{A}| = 0, \quad \text{then} \quad |A_0| = |A_1|. \quad (3.28)$$

Although the moduli $|A_0|$ and $|A_1|$ are unknown, the physical values of $\cos(\phi - \bar{\phi})$ impose bounds:

$$\frac{1}{\sqrt{2}}\| |A| - |\bar{A}| \| \leq |A_n| \leq \frac{1}{\sqrt{2}}(|A| + |\bar{A}|), \quad (3.29)$$

where $n = 0, 1$. The bounds (3.29) can be narrowed given the sign of $\cos(\phi - \bar{\phi})$. For instance, with $\cos(\phi - \bar{\phi}) > 0$, we have

$$\begin{aligned} \sqrt{\frac{1}{2}\sigma_A} < |A_0| \leq \frac{1}{\sqrt{2}}(|A| + |\bar{A}|), \\ \frac{1}{\sqrt{2}}||A| - |\bar{A}|| \leq |A_1| < \sqrt{\frac{1}{2}\sigma_A}. \end{aligned} \quad (3.30)$$

For $\cos(\bar{\phi} - \phi) < 0$, the positions of moduli $|A_0|$ and $|A_1|$ in the inequalities (3.30) are reversed.

IV. RESULTS

In the Saclay experiment, the spin-density-matrix elements (2.6) were obtained using the usual method of unconstrained optimization of maximum-likelihood function in experimental data analysis. For both incident momenta of 5.98 and 11.85 GeV/c, the amplitude analysis was performed in two distinct kinematic regions:

$$0.1 \leq |t| \leq 1.0 \text{ (GeV/c)}^2, \quad 720 \leq m \leq 820 \text{ MeV}, \quad (4.1)$$

$$0.2 \leq |t| \leq 0.4 \text{ (GeV/c)}^2, \quad 360 \leq m \leq 1040 \text{ MeV}. \quad (4.2)$$

There are 7 t bins in (4.1) to study the t dependence of moduli and cosines at fixed mass interval near ρ^0 mass. In (4.2) there are 12 mass bins to study the mass dependence of the same amplitudes in the fixed interval of $-t$. In each case the amplitude analysis was carried out in both s - and t -channel helicity frames for the meson system.

The first run of amplitude analysis produced solutions of cubic equations for $|L|^2$ and $|\bar{L}|^2$ which were all real in some (m, t) bins. In other bins at least one of moduli $|L|^2$ and $|\bar{L}|^2$ had a complex solution. The (m, t) bins with complex solutions were subjected to secondary runs with small modifications of observables, within errors, to satisfy a subset of linear inequalities from (3.19) and to yield real solutions while minimizing a χ^2 function.

In each (m, t) bin one of the solutions is large and negative, and it is rejected (solution 3 of Table I). The remaining two real and positive solutions are labeled solution 1 and solution 2, with solution 1 being the larger of the two in agreement with (3.14). In some cases the solutions lead to small negative values of other moduli, or to cosines with absolute values larger than 1. In general, these results are still compatible with physical values within errors, and left unchanged.

In certain cases, especially at 11.85 GeV/c, we have not obtained real solutions by small modifications of input data in the vicinity of their original mean values. In such cases we accept the real part of the complex-conjugate solutions as an approximate double solution labeled solution 0. This procedure is justified by the fact that the imaginary parts are, in general, small.

The experimental data analysis used optimization program FUMILI [56] and the produced error matrix was used in error calculations in the amplitude analysis. A linear approximation for error propagation was used to evaluate errors on solutions of the cubic equations. We believe that this procedure tends to overestimate the final

errors on moduli and cosines in many cases.

In the following figures, the results for solutions 1 and 2 are represented by symbols + and ●, respectively. Solution 0 is represented by symbol ○ without error bars. The errors on solution 0 are comparable to errors on nearby real solutions. The figures for cosines do not show some results with unphysical values.

Using the ordering of (3.14), we now denote the two solutions for transversity amplitudes as $A(i)$ and $\bar{A}(j)$ with $i=1,2$ and $j=1,2$. The solutions for the two groups of amplitudes with opposite transversities given by (2.21) and (2.22) are entirely independent. As the result, there is a fourfold ambiguity in the partial-wave cross sections and polarizations. Using the above indices i and j to label the four solutions, we get

$$\begin{aligned} \sigma(A) &\equiv \sigma_A(i, j) = |A(i)|^2 + |\bar{A}(j)|^2, \\ \tau(A) &\equiv \tau_A(i, j) = |A(i)|^2 - |\bar{A}(j)|^2. \end{aligned} \quad (4.3)$$

Then for $A=L, U, N$,

$$\begin{aligned} \sigma_A(1, 1) \geq \sigma_A(1, 2), \quad \sigma_A(2, 1) \geq \sigma_A(2, 2), \\ \tau_A(1, 2) \geq \tau_A(1, 1), \quad \tau_A(2, 2) \geq \tau_A(2, 1). \end{aligned} \quad (4.4)$$

For $A=S$, all inequality signs in (4.4) are reversed. There are four solutions for the unnormalized partial-wave cross sections:

$$I_A(i, j) = \sigma_A(i, j) \Sigma, \quad (4.5)$$

where Σ is the reaction cross section.

A. t dependence of solutions in the mass region of ρ^0 resonance

Our results for the moduli of nucleon transversity amplitudes and the cosines of relative phases in the kinematic region $0.1 \leq |t| \leq 1.0 \text{ (GeV/c)}^2$ and $720 \leq m \leq 820 \text{ MeV}$ are shown in Figs. 1 and 2 for $p_{\text{lab}} = 5.98$ and 11.85 GeV/c, respectively. Each figure shows the results of independent analysis in the t - and s -channel helicity frames. Figure 3 shows the partial-wave polarizations $\tau(1,2)$ and $\tau(2,1)$ at 5.98 GeV/c. The solutions $\tau(1,1)$ and $\tau(2,2)$ are within the bounds of $\tau(1,2)$ and $\tau(2,1)$ and show similar behavior.

In the t -channel helicity frame, the $\pi^+ \pi^-$ production at small t is dominated by the amplitude $|\bar{L}|^2$, and the $\pi^+ \pi^-$ state is thus produced predominantly with longitudinal helicity $\lambda=0$. The decrease of $|\bar{L}|^2$ with increasing momentum transfer is compensated by the increase in amplitudes $|\bar{U}|^2$ and especially $|\bar{N}|^2$, which dominates the $\pi^+ \pi^-$ production at larger t . There is also an increase of $|\bar{S}|^2$ with t in solution 2. This behavior of the moduli gives rise to a crossover for the amplitudes with opposite transversities. From Fig. 3 we observe that $|S| = |\bar{S}|$ for $-t = 0.45 - 0.55 \text{ (GeV/c)}^2$, $|L| = |\bar{L}|$ at $-t \approx 0.6 \text{ (GeV/c)}^2$, $|U| = |\bar{U}|$ at $-t \approx 0.5 \text{ (GeV/c)}^2$ and $|N| = |\bar{N}|$ near $-t \approx -0.5 \text{ (GeV/c)}^2$. For $-t \leq 0.25 \text{ (GeV/c)}^2$ and $-t \geq 0.4 \text{ (GeV/c)}^2$, the $\pi^+ \pi^-$ production proceeds predominantly with recoil nucleon spin "up."

In $\pi N \rightarrow \pi^+ \pi^- N$ reactions, the helicity amplitudes S_0, L_0, U_0 and S_1, L_1, U_1 are associated with t -channel ex-

change quantum numbers of A_1 and π mesons, respectively. The large differences between $|L|^2$ and $|\bar{L}|^2$ for $-t \leq 0.5$ and $|S|^2$ and $|\bar{S}|^2$ for $-t \geq 0.5$ are a clear signal for strong and nontrivial “ A_1 ” exchange contributions with phases different from the “ π ” exchange amplitudes.

A comparison of the behavior of τ_S , τ_L , and τ_U in Fig. 3 indicates that the corresponding pairs of “ A_1 ” and “ π ” exchange amplitudes have nonsimilar relative phases which change signs at the crossover points.

The helicity amplitudes N_0 and N_1 both exchange A_2

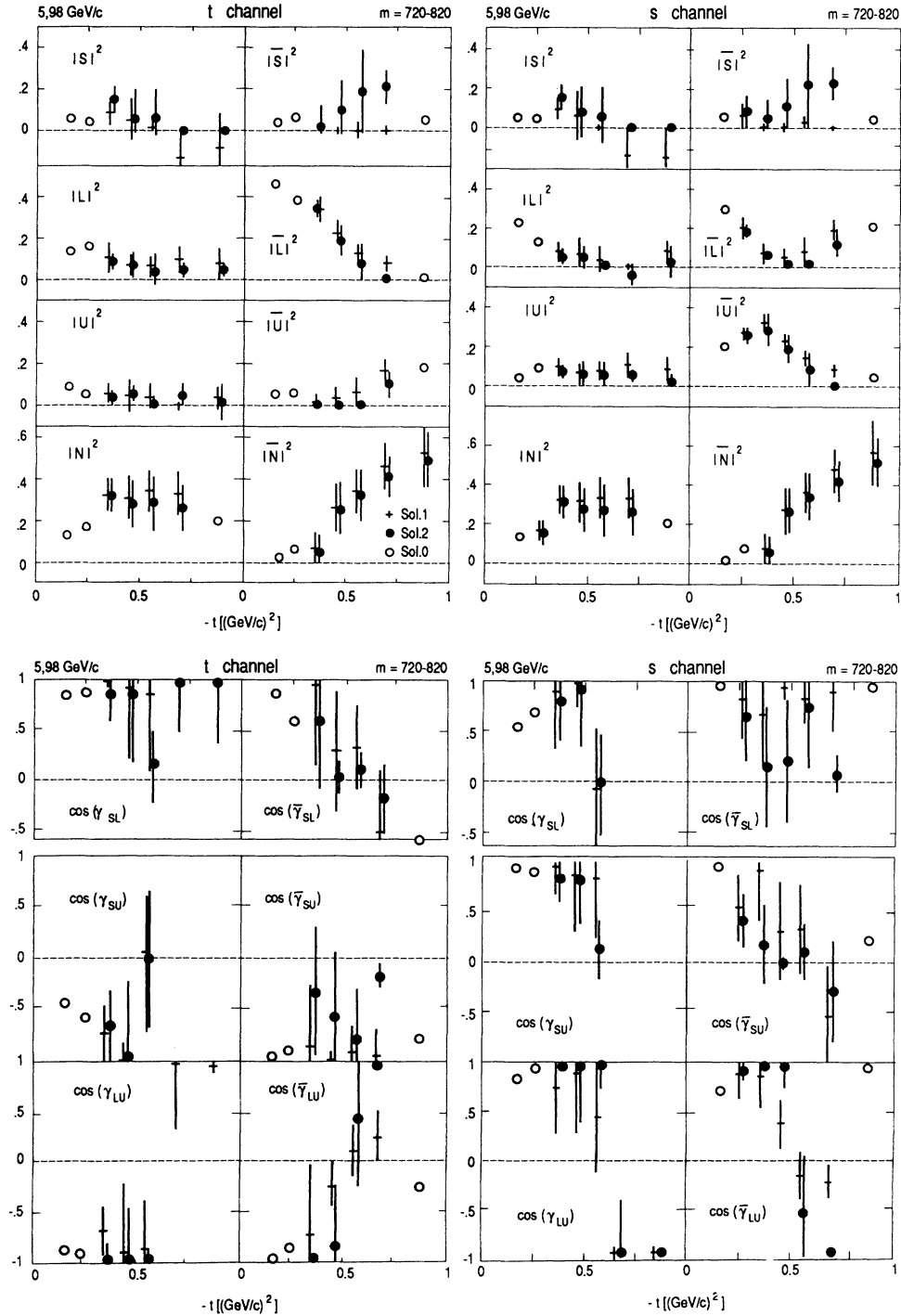


FIG. 1. The t dependence of moduli squared of normalized nucleon transversity amplitudes and cosines of their relative phases for dimeson masses in ρ^0 mass region $m = 720\text{--}820$ MeV at π^+ incident momentum of 5.98 GeV/c. The symbols +, ●, and ○ denote solution 1, solution 2, and solution 0 (real part of complex solution), respectively.

quantum numbers. The crossing of $|N|^2$ and $|\bar{N}|^2$ near $-t \approx 0.5$ (GeV/c)² is due to the change of sign in the relative phase of N_0 and N_1 . We find a similar crossover of $|N|^2$ and $|\bar{N}|^2$ also at 11.85 GeV/c (Fig. 2). We note that the data on polarization in $\pi^- p \rightarrow \eta n$ at 7.85 GeV/c, a reaction which proceeds by pure “ A_2 ” exchange, also show such change of sign [57]. The construction [7,8] of “ A_2 ”

exchange amplitudes from KN and $\bar{K}N$ charge-exchange data at 6 GeV/c produces a nonflip amplitude with $\text{Re}N_0$ changing sign and $\text{Im}N_0$ having a double zero in the interval $-t \approx 0.4-0.5$ (GeV/c)². The same conclusion was reached from a simultaneous analysis [58] of reactions $\pi^- p \rightarrow \pi^0 n$, $\pi^- p \rightarrow \eta n$, and $K^- p \rightarrow \bar{K}^0 n$ at 6 GeV/c. Our data suggest that N_0 in $\pi^+ n \rightarrow \pi^+ \pi^- p$ has a similar

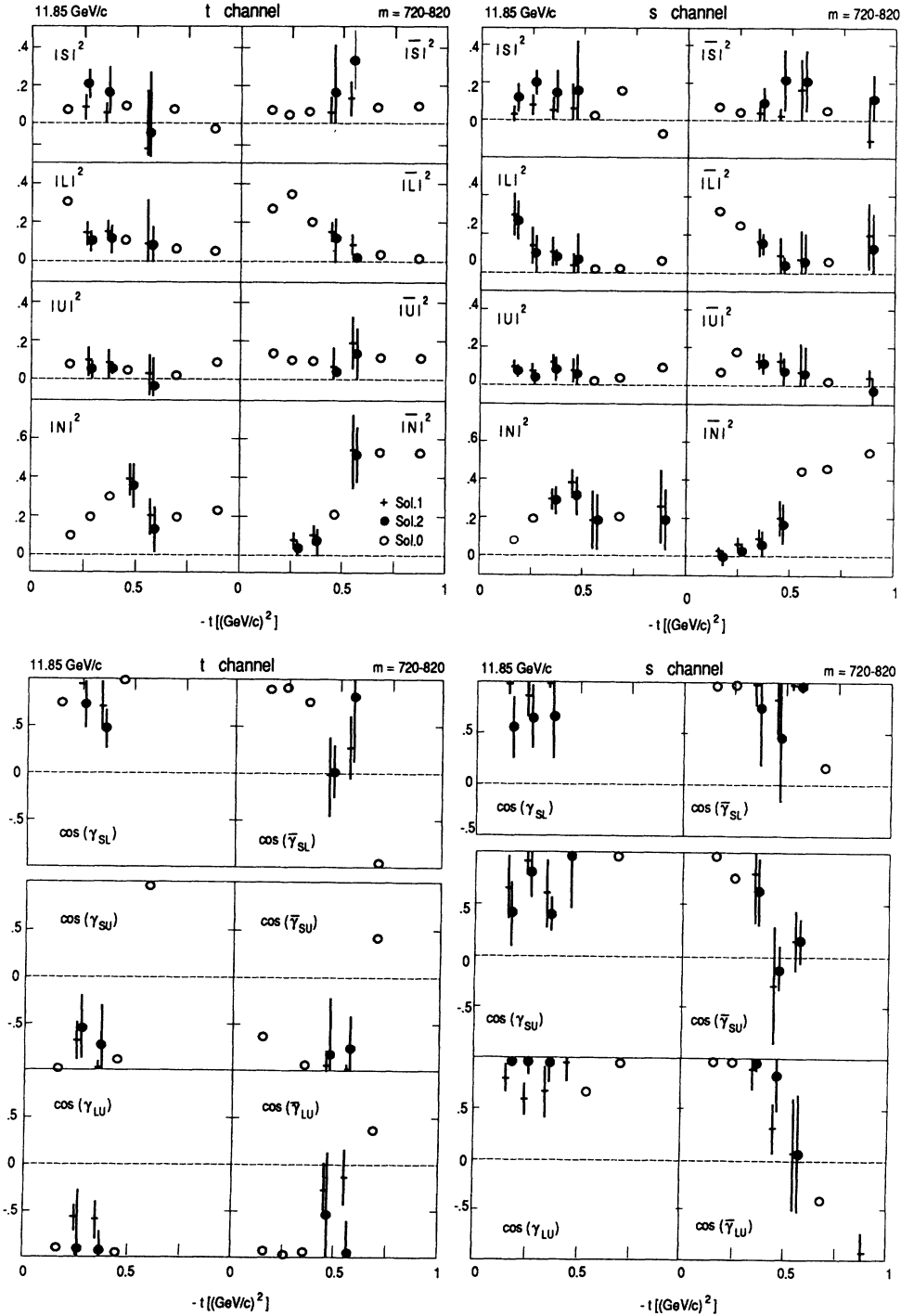


FIG. 2. The t dependence of moduli squared of normalized nucleon transversity amplitude and cosines of their relative phases for dimeson masses in ρ^0 mass region $m = 720-820$ MeV at π^+ incident momentum of 11.85 GeV/c. The symbols are as in Fig. 1.

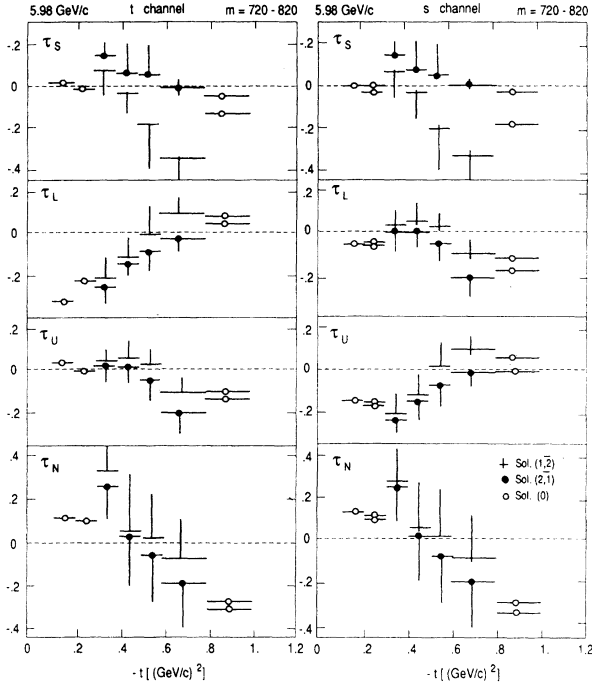


FIG. 3. The t dependence of partial-wave recoil nucleon polarizations τ in ρ^0 mass region $m = 720\text{--}820$ MeV at incident π^+ momentum of 5.98 GeV/c in the dimeson t - and s -channel helicity frames.

structure.

The relative phases between transversity amplitudes exhibit similar behavior for both solutions. The amplitudes S and L appear approximately in phase, while \bar{S} and \bar{L} have their phases diverging nearly by 180° with increasing $-t$ and with their relative phase passing through 90° at $-t \approx 0.6$ (GeV/c) 2 . The relative phases γ_{LU} and $\bar{\gamma}_{LU}$ both undergo a 180° change from near $\pm 180^\circ$ to near 0° , passing through $\pm 90^\circ$ at $-t \approx 0.6$. While the phases of \bar{S} and \bar{L} diverge, the phases of L and U , and \bar{L} and \bar{U} converge with increasing $-t$ for $-t \lesssim 1.0$ (GeV/c) 2 . The amplitudes \bar{S} and \bar{U} appear approximately 180° out of phase, at least for solution 1.

The results at 11.85 GeV/c in the t -channel helicity frame (Fig. 2) are similar to those at 5.98 (GeV/c). There is some indication for a smaller contribution by $|\bar{L}|^2$ and larger contributions by $|\bar{S}|^2$ and $|\bar{U}|^2$. This would indicate that the effective Regge trajectories of the normalized amplitudes $|\bar{L}|^2$ and $|\bar{S}|^2$, $|\bar{U}|^2$ are negative and positive, respectively. We also observe the crossover between $|N|^2$ and $|\bar{N}|^2$ at $-t \approx 0.5$ as in data at 5.98 GeV/c.

Our results in the t channel can be compared with the results of amplitude analysis of $\pi^- p \rightarrow \pi^- \pi^+ n$ at 17.2 GeV/c, also performed in the t channel in the ρ^0 mass region of $710 \leq m \leq 830$ MeV and $0 < -t < 1.0$ (GeV/c) 2 (Figs. 8 and 9 in Ref. [18]). In the kinematic region of overlap, we find a qualitative agreement but also some interesting differences. In particular, solution 2 for the $|\bar{S}|^2$ amplitude is substantially larger at 5.98 and 11.85 GeV/c than both solutions for $|\bar{S}|^2$ at 17.2 GeV/c. There is also no crossover of $|N|^2$ and $|\bar{N}|^2$ at $-t \approx 0.5$ (GeV/c) 2 , but

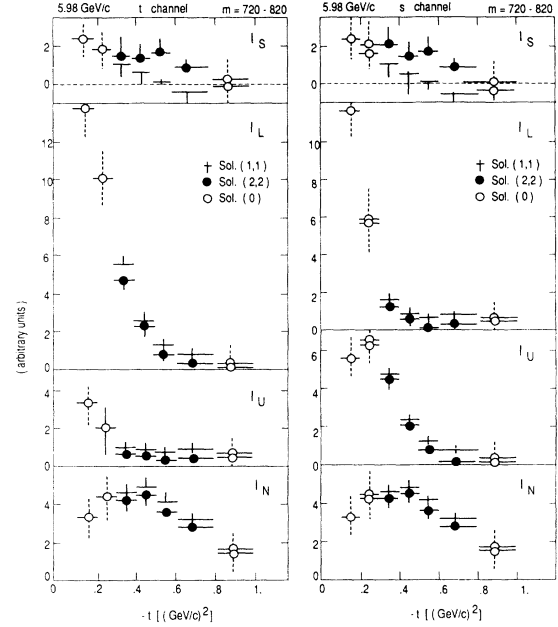


FIG. 4. The t dependence of unnormalized partial-wave cross sections in ρ^0 mass region $m = 720\text{--}820$ MeV at incident π^+ momentum of 5.98 GeV/c in the dimeson t - and s -channel helicity frames of reference. The units are arbitrary but are the same in both helicity frames.

it may occur near $-t \approx 0.7\text{--}0.8$ (GeV/c) 2 . The amplitudes $|N|^2$ and $|\bar{N}|^2$ have a different behavior and relative magnitudes at 17.2 GeV/c in comparison with 5.98 GeV/c. The relative phases γ_{SL} , $\bar{\gamma}_{SL}$, and $\bar{\gamma}_{LU}$ are very similar at 5.98 and 17.2 GeV/c, but γ_{LU} appears constant at 17.2 GeV without the 180° change seen at 5.98 GeV/c.

The moduli $|S|^2$, $|\bar{S}|^2$, $|N|^2$, and $|\bar{N}|^2$ are helicity frame invariant. A comparison of our results in the t - and s -channel helicity frames in Figs. 1–3 confirms this expectation. We also notice that, in our kinematic region, the t - to s -channel crossing is approximately equal to a change of $L \rightarrow +U$ and $U \rightarrow -L$.

To calculate the unnormalized partial-wave cross sections $I_A(i,j)$, $A = S, L, U, N$ and $i, j = 1, 2$, we have used for the reaction cross section Σ an estimate based on our experiment and described in Ref. [29]. The solutions $I_A(1,1)$ and $I_A(2,2)$, $A = S, L, U, N$, are presented in Fig. 4. The behavior of I_L shows the expected forward peak due to the pion-exchange dominance. The forward behavior of I_U in the s channel reveals the importance of helicity-flip amplitude U_1 in the s channel. The rather flat slope of I_S counter indicates a strong influence of the nearby pion pole in the helicity-flip amplitude S_1 . The solution $I_S(2,2)$ may have a dip at $-t \approx 0.45$ (GeV/c) 2 . The cross section on I_N peaks at $-t \approx 0.45$ (GeV/c) 2 , and its behavior at smaller $-t$ suggest a dominant contribution of helicity-flip amplitude N_1 , or a possible dip at $-t \approx -0.15$ (GeV/c) 2 . The shape of I_N at 5.98 GeV/c is substantially different from the cross section for $\pi^- p \rightarrow \eta n$ at 6 GeV/c (see Fig. 13 in Ref. [8]), a process which is also dominated by pure “ A_2 ” exchange helicity amplitudes.

**B. The mass dependence of solutions
for $-t=0.2-0.4$ (GeV/c)²**

The mass dependence of the moduli of NTA and cosines of relative phases in the mass interval $m=360-1040$ MeV and in the single t bin $-t=0.2-0.4$ (GeV/c)² is shown in Figs. 5–8. Again, we present the

results of independent analyses in the t - and s -channel helicity frames at both incoming momenta of 5.98 and 11.85 GeV/c. In Fig. 9 we present partial-wave polarizations $\tau(1,2)$ and $\tau(2,1)$ at 5.98 GeV/c for both helicity frames.

First we discuss our results in the t channel. Solutions 1 and 2 are rather similar with the exception of $|\bar{S}|^2$ for

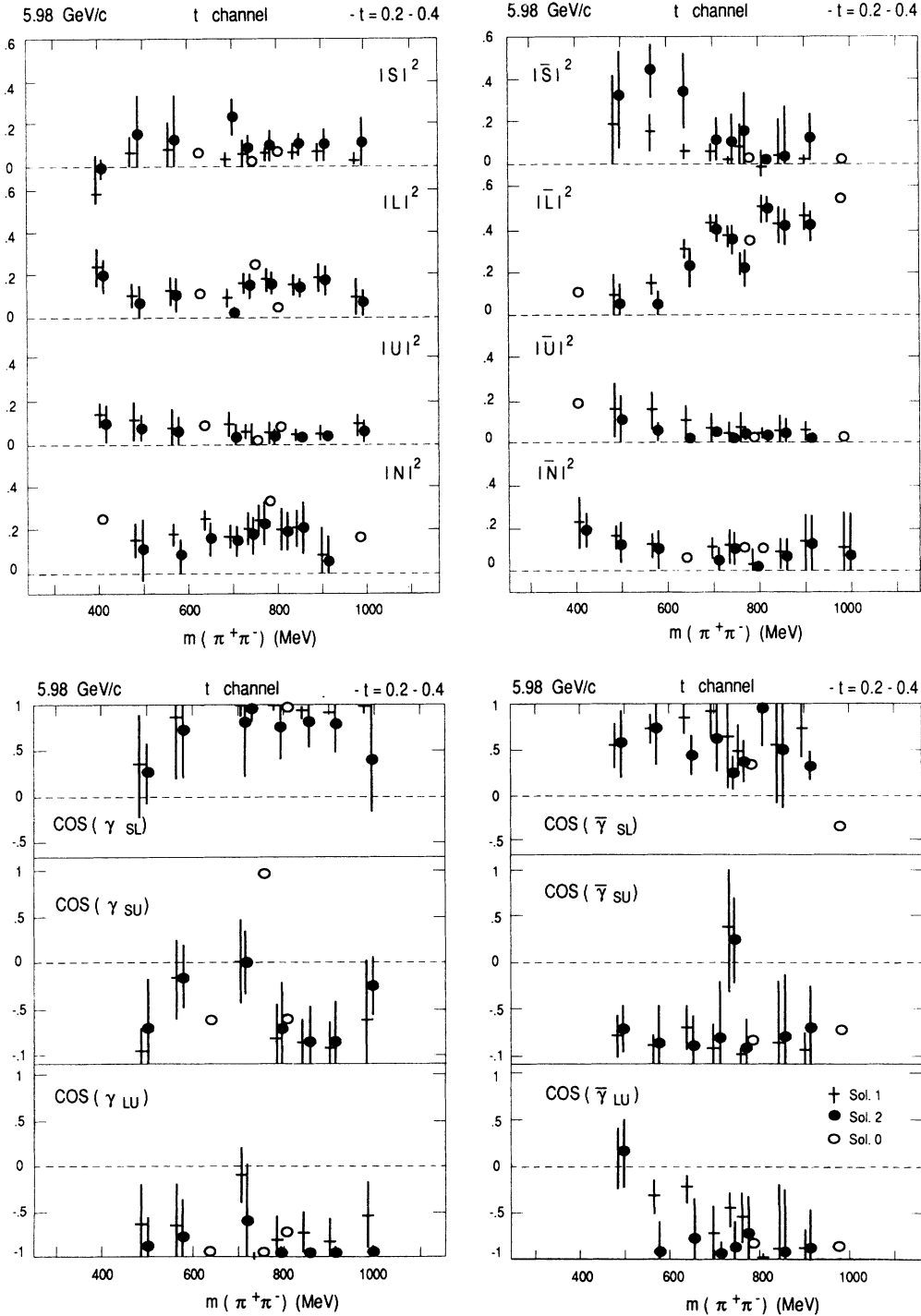


FIG. 5. The m dependence of moduli squared of normalized nucleon transversity amplitude and cosines of their relative phases for momentum transfer $-t=0.2-0.4$ (GeV/c)² at 5.98 GeV/c in the dimeson t -channel helicity frame of reference. The symbols are as in Fig. 1.

$m \leq 650$ MeV where solution 2 is larger than solution 1 by a factor of 2–3. For $m \geq 800$ MeV, the amplitude $|\bar{L}|^2$ dominates and accounts for $\sim 50\%$ of the $\pi^+\pi^-$ production. Particularly noteworthy are the structures of moduli $|L|^2$ and $|\bar{L}|^2$ and $|N|^2$ and $|\bar{N}|^2$ within the mass range of the ρ^0 resonance.

The amplitude $|L|^2$ peaks at 760 MeV while $|\bar{L}|^2$ dips. Moreover, at this mass $|L|^2 \approx |\bar{L}|^2$, as seen from the be-

havior of τ_L . For $m \geq 600$ MeV, the relative phase $\phi_{L_0} - \phi_{L_1}$ is negative and vanishes at 760 MeV. Alternatively, $|L_0|^2$ or $|L_1|^2$ varies rapidly within the resonance width and vanishes at 760 MeV.

The amplitude $|N|^2$ peaks at 780 MeV while $|\bar{N}|^2$ dips to $|\bar{N}|^2 \approx 0$ at the same mass. Thus, $|N_0|^2 \approx |N_1|^2$ at $m \approx 780$ MeV and for $-t = 0.2 - 0.4$ (GeV/c)². We note that “ A_2 ” exchange helicity amplitudes in KN charge ex-

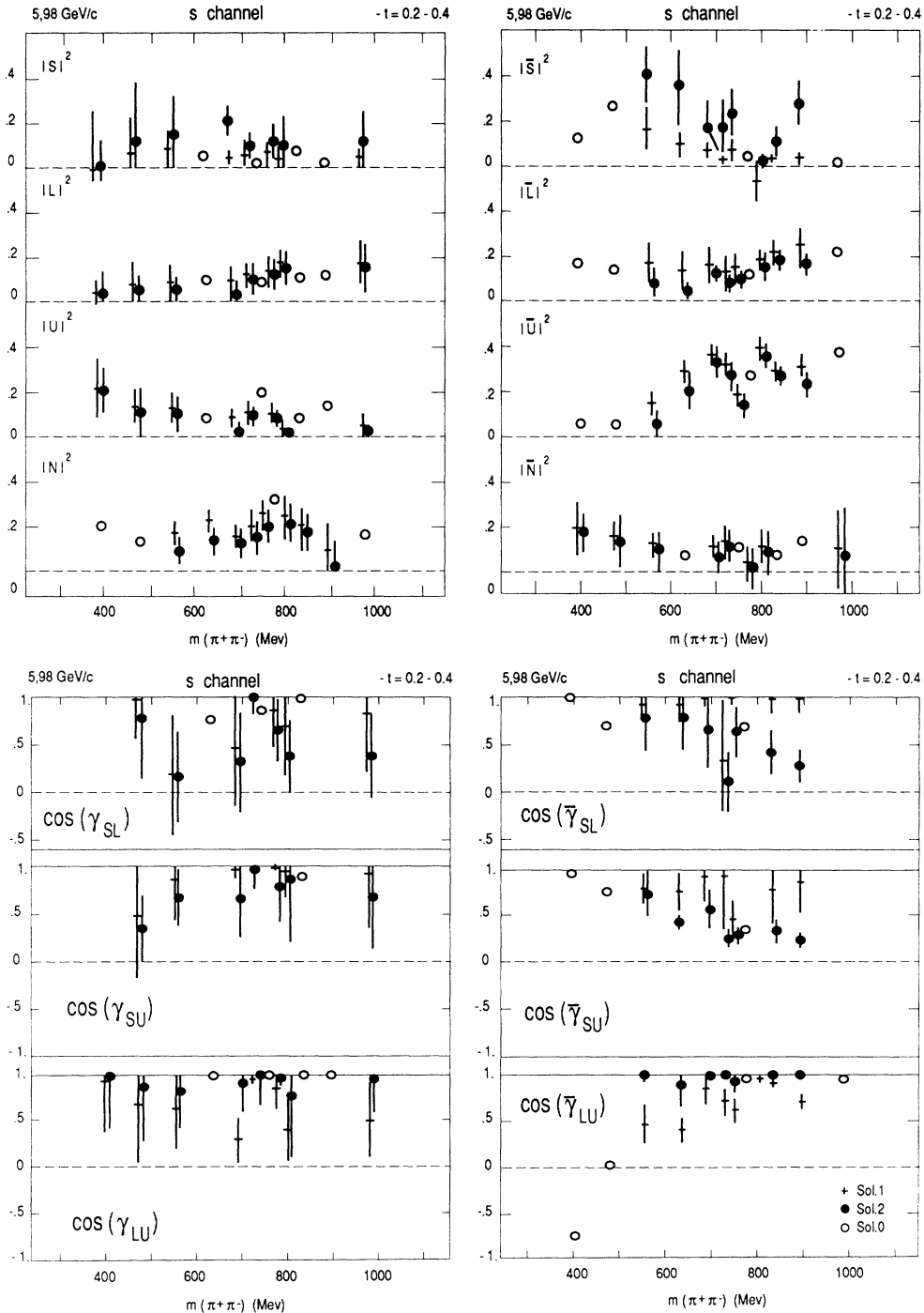


FIG. 6. Same as Fig. 5 in the dimeson s -channel helicity frame of reference.

change at the same energy and momentum transfer have different structure with $|N_1|^2$ larger than $|N_0|^2$.

The amplitudes $|U|^2$ and $|\bar{U}|^2$ show a smooth behavior. Their small magnitudes indicate that the $\pi^+ \pi^-$ state with transverse dipion helicities $\lambda = \pm 1$ is produced mostly through natural exchange at this range of $-t$. However, the situation is different in the s -channel helicity frame. There it is the amplitude $|\bar{U}|^2$ which dominates and dips

at $m \approx 760$ MeV while $|U|^2$ peaks at this mass and $|L|^2$ and $|\bar{L}|^2$ appear structureless. The rapid variations in magnitude of amplitudes U , \bar{U} , N , and \bar{N} within the ρ^0 mass region reflect rapid changes in magnitudes and/or phases of the corresponding helicity amplitudes with transverse dipion helicity $\lambda = \pm 1$ in the s -channel helicity frame.

The large differences in magnitude and behavior be-

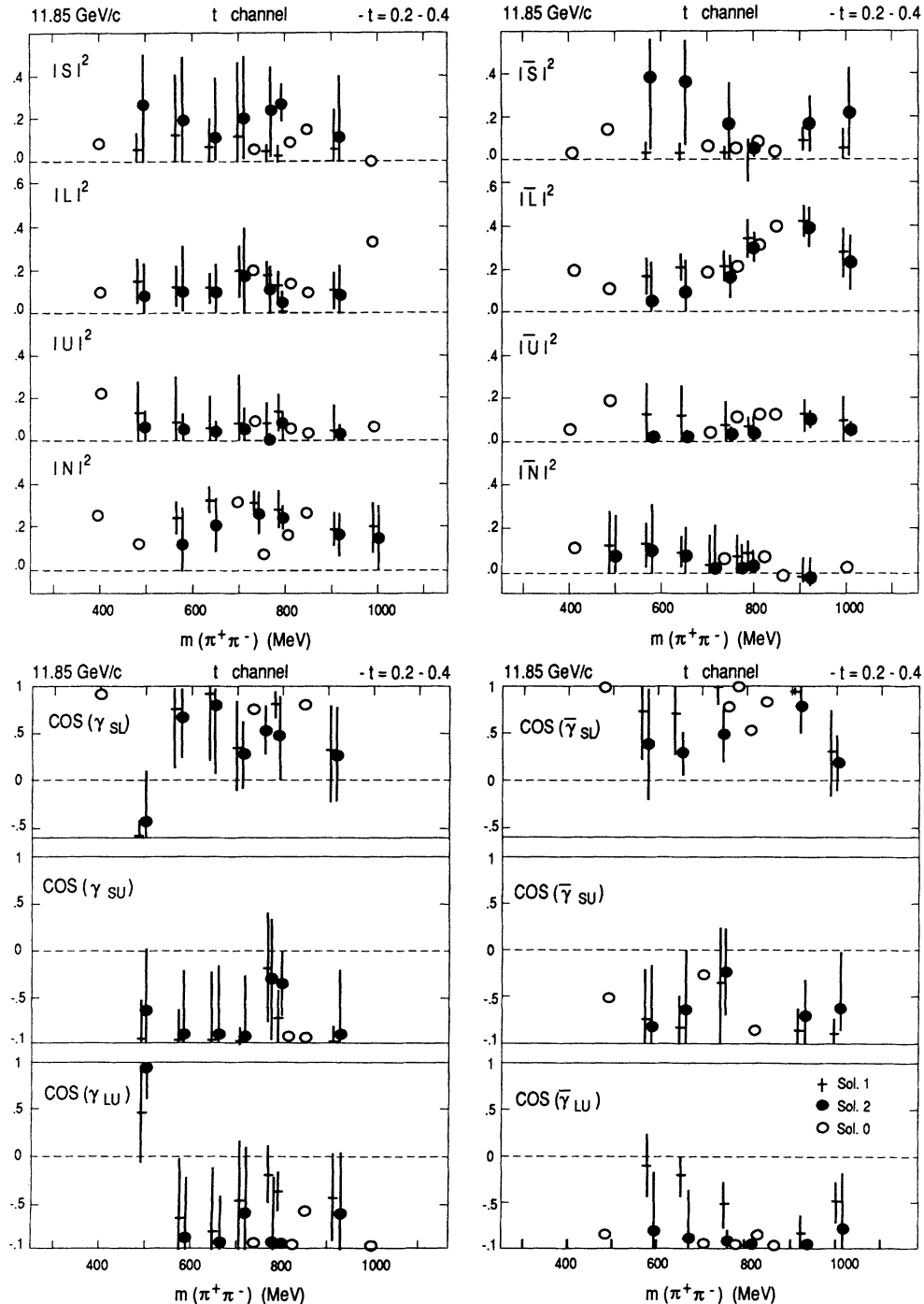


FIG. 7. The m dependence of moduli squared of normalized nucleon transversity amplitudes and cosines of their relative phases for momentum transfers $-t = 0.2 - 0.4$ (GeV/c)² at 11.85 GeV/c in the dimeson t -channel helicity frame. The symbols are as in Fig. 1.

tween the amplitudes $|\bar{L}|^2$ and $|L|^2$ in the t channel and between $|\bar{U}|^2$ and $|U|^2$ in the s channel for masses $m \geq 600$ MeV are a clear signal for large and nontrivial “ A_1 ” exchange nonflip amplitudes L_0 and U_0 in the ρ^0 mass region. The “ A_1 ” exchange also contributes to $\pi^+\pi^-$ production in the $J=0$ spin state, and for $-t=0.2-0.4$ (GeV/c)² its contribution to the S -wave amplitude S_0 is large for masses $m \leq 700$ MeV. The

differences in partial-wave polarizations $\tau_S, \tau_L,$ and τ_U in each frame indicate that the associated pairs of “ A_1 ” and “ π ” exchange amplitudes $S_0, S_1, L_0, L_1,$ and U_0, U_1 have dissimilar behavior. The detailed structures of these “ A_1 ” and “ π ” exchange amplitudes thus also depend on the spin and helicity of the $\pi^+\pi^-$ state. The behavior of τ_N indicates a rapidly varying relative phase of the two “ A_2 ” exchange amplitudes N_0 and N_1 within the ρ^0 reso-

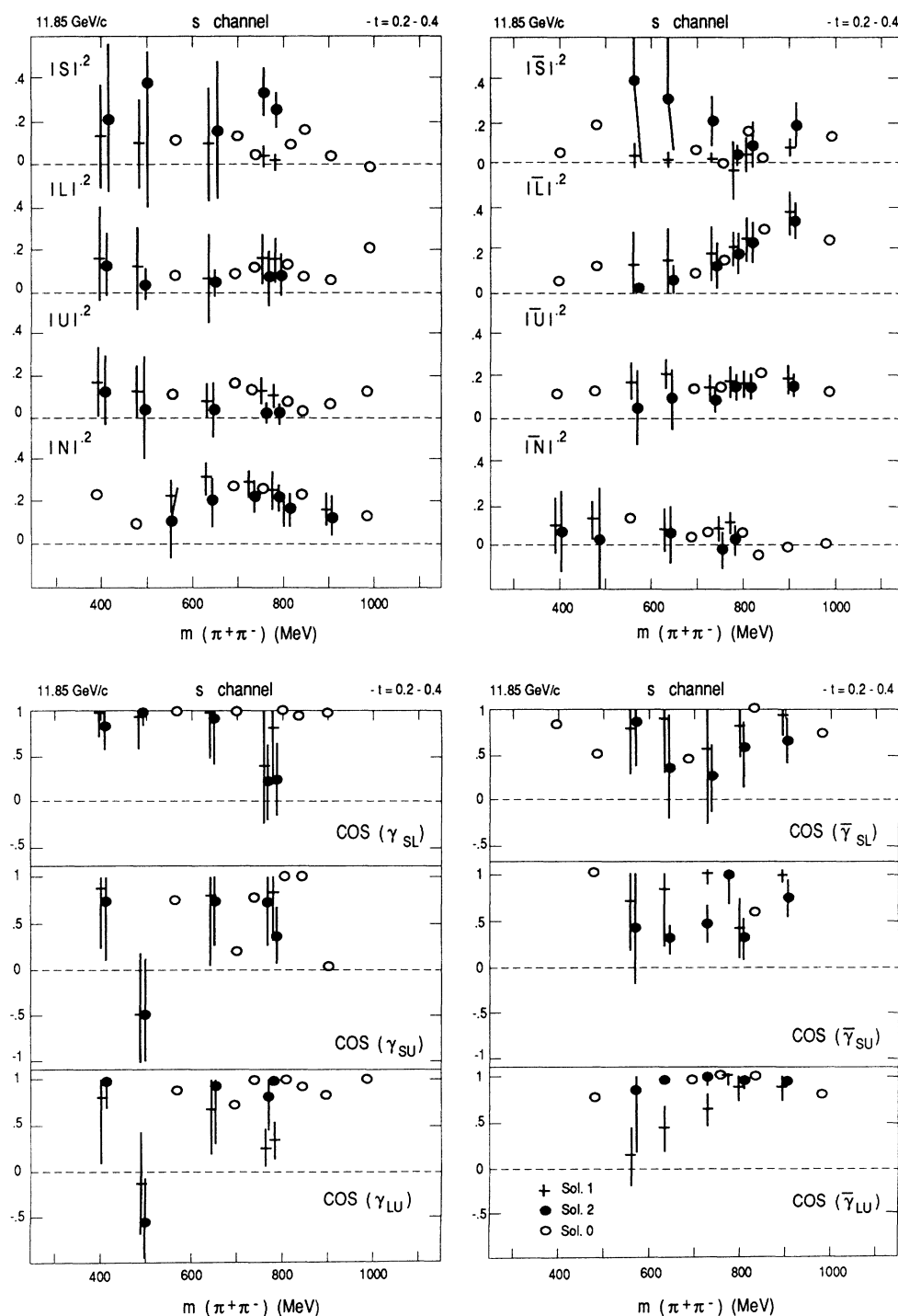


FIG. 8. Same as Fig. 7 in the dimeson s -channel helicity frame.

nance mass region.

The results at 11.85 GeV/c are similar with one noticeable exception. Although the amplitudes $|\bar{L}|^2$ in the t channel and $|\bar{U}|^2$ in the s channel both increase with dipion mass m , there is no apparent dip at 760 MeV as seen

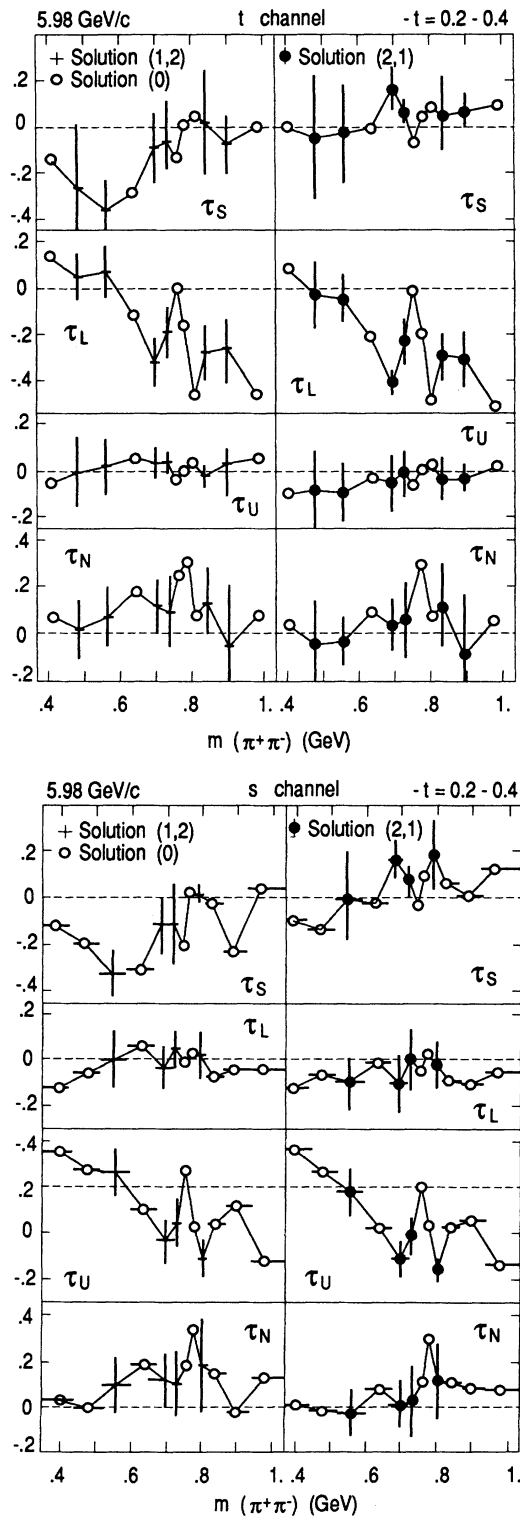


FIG. 9. The m -dependence of partial-wave recoil nucleon polarizations τ for $-t=0.2-0.4$ (GeV/c)² at 5.98 GeV/c in the dimeson t - and s -channel helicity frames.

at 5.98 GeV/c. There is a possibility that the dip is shifted to larger $-t$ (see Fig. 15 below). We also note that systematic errors are larger at this energy.

In Fig. 10 we present unnormalized partial-wave cross sections $I_A(1,1)$ and $I_A(2,2)$, $A=S,L,U,N$ in the s chan-

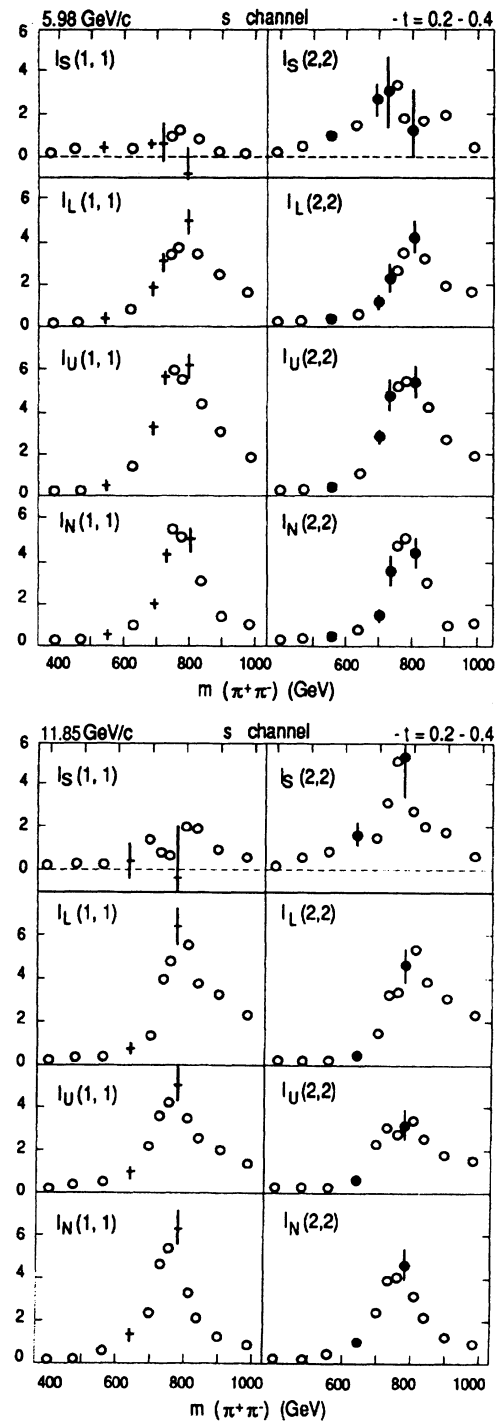


FIG. 10. The m dependence of unnormalized partial-wave cross sections for $-t=0.2-0.4$ (GeV/c)² at π^+ incident momenta of 5.98 and 11.85 GeV/c in the dimeson s -channel helicity frame. The units are arbitrary and are different at each incident momentum.

nel at both energies. For the reaction cross sections we have again used estimates based on the Saclay experiment [29]. The spin-averaged P -wave cross sections I_L , I_U , and I_N show ρ_0 resonance peaks which give no hint of any underlying structures within the resonance width seen on the level of production amplitudes. We notice, however, that in both solutions the apparent width of the ρ_0 peak in I_N is narrower than the widths of the peaks in I_U and I_L .

The S -wave cross sections, in particular $I_S(2,2)$, show a peak at ~ 750 MeV. The smooth behavior of the normalized amplitude $|S|^2$ and of its relative phase γ_{SU} with a large-amplitude U resonating a nearby mass (Fig. 6), indicates a resonant behavior of the amplitude S corresponding to a scalar state $I=00^{++}(750)$ (see also Refs. [35,36]). This aspect of our amplitude analysis will be discussed in a greater detail elsewhere.

C. Verification of the method of analysis

The moduli $|S|^2$, $|\bar{S}|^2$, $|N|^2$ and $|\bar{N}|^2$ are helicity frame invariant. The data analysis as well as the amplitude analyses were carried out independently in the s - and t -channel helicity frames. The results confirm the expected helicity frame invariance of these moduli. This confirmation provides an important self-consistency test of our amplitude analysis.

A potential difficulty stems from the fact that the input SDM elements are not exact but bin-averaged values. The nonlinear equations for moduli (3.13) apply, strictly speaking, only to the point values of SDM elements. While bin-averaged SDM elements will continue to satisfy any linear relations among these observables, nonlinear relations will not be exactly satisfied. Using nonlinear relations to calculate amplitudes from bin-averaged data will introduce necessarily distortions in the results. We would like to know if the distortions could be large enough so that they can modify the interpretations of our results.

Any answer to such a question coming from the same set of input data on SDM elements must necessarily involve linear relations. Such a self-test for nonlinear distortions is provided by bounds on moduli $|A|^2$ and $|\bar{A}|^2$, $A=S, L, U, N$. The linear equations (3.2) determine mixed combinations of moduli squared:

$$\begin{aligned} |L|^2 + \frac{1}{3}|S|^2, \quad |U|^2 + \frac{1}{3}|S|^2, \quad |\bar{N}|^2 + \frac{1}{3}|S|^2, \\ |\bar{L}|^2 + \frac{1}{3}|\bar{S}|^2, \quad |\bar{U}|^2 + \frac{1}{3}|\bar{S}|^2, \quad |N|^2 + \frac{1}{3}|\bar{S}|^2. \end{aligned} \quad (4.6)$$

The results (4.6) represent upper bounds $|A|_{\text{upper}}^2$, $|\bar{A}|_{\text{upper}}^2$ on the moduli squared of P -wave amplitudes corresponding to the absence of the S wave:

$$|S|_{\text{lower}}^2 = |\bar{S}|_{\text{lower}}^2 = 0. \quad (4.7)$$

The lower bounds on P -wave moduli are obtained by subtracting from each term in (4.6) an upper bound on $\frac{1}{3}|S|^2$ and $\frac{1}{3}|\bar{S}|^2$. Since amplitudes S , \bar{S} , N , and \bar{N} are invariant under s - to t -channel helicity frame transformation, we calculate, in each (m, t) bin,

$$\begin{aligned} \left(\frac{1}{3}|S|^2\right)_{\text{upper}} &= \min_{\substack{A=L,U \\ s \text{ and } t}} \{ |A|^2 + \frac{1}{3}|S|^2, |\bar{N}|^2 + \frac{1}{3}|S|^2 \}, \\ \left(\frac{1}{3}|\bar{S}|^2\right)_{\text{upper}} &= \min_{\substack{A=L,U \\ s \text{ and } t}} \{ |\bar{A}|^2 + \frac{1}{3}|\bar{S}|^2, |N|^2 + \frac{1}{3}|\bar{S}|^2 \}. \end{aligned} \quad (4.8)$$

Lower bounds on P -wave moduli are then

$$\begin{aligned} |A|_{\text{lower}}^2 &= |A|_{\text{upper}}^2 - \left(\frac{1}{3}|S|^2\right)_{\text{upper}} \\ |\bar{A}|_{\text{lower}}^2 &= |\bar{A}|_{\text{upper}}^2 - \left(\frac{1}{3}|\bar{S}|^2\right)_{\text{upper}}. \end{aligned} \quad (4.9)$$

The bounds calculated for (t, m) bins in the kinematic regions (4.1) and (4.2) were reported previously in Ref. [29]. For convenience of comparison, we present these results at 5.98 GeV/c in Figs. 11 and 12.

The bounds are most restrictive for the P -wave moduli. We note that the mean values of both solutions obtained for the moduli in our amplitude analysis are contained, in general, within the bounds. The bounds show the same structural features exhibited by the solutions; in particular, they show the structures within the mass interval of the ρ_0 width. We conclude that the nonlinear distortions are small on our level of statistics.

The bounds in Figs. 11 and 12 were shown without errors for the sake of clarity. In Figs. 13 and 14 we show statistical errors on bounds for several interesting structures in the dependence on momentum transfer t and mass m , respectively (see also Fig. 4 of Ref. [38]). We conclude that the observed spin-dependent behavior of moduli and the structures near the ρ_0 mass are statistically significant and are unaffected by the presence of small nonlinear distortions.

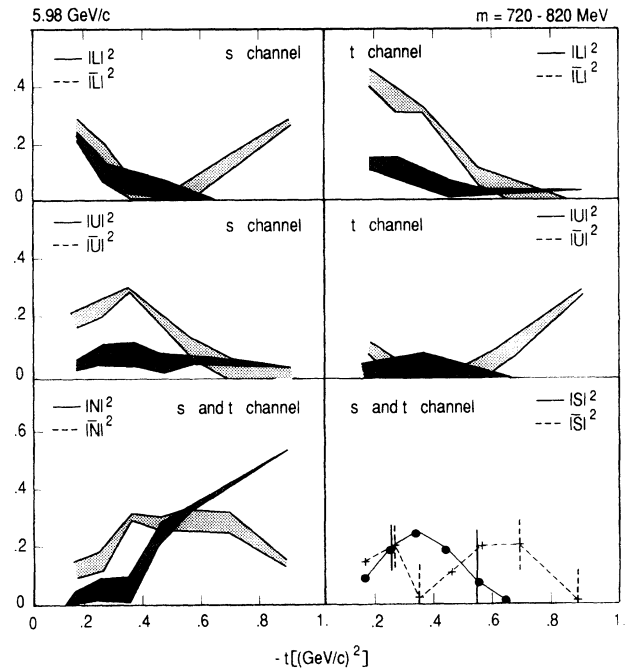


FIG. 11. The t dependence of the lower and upper bounds on the moduli squared of the normalized P -wave nucleon transversity amplitudes for $m=720-820$ MeV at 5.98 GeV/c. Also shown are the upper bounds for the normalized S -wave amplitudes.

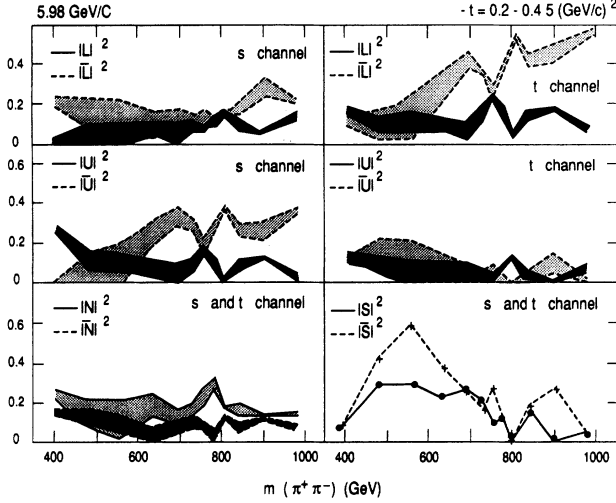


FIG. 12. The m dependence of the lower and upper bounds on the moduli squared of the normalized P -wave nucleon transversity amplitudes for $-t=0.2-0.4$ (GeV/c)² at 5.98 GeV/c , and the upper bounds for the S -wave normalized moduli squared.

V. DISCUSSION

The pion production process $\pi N \rightarrow \pi\pi N$ has always served to develop our ideas on dynamics of hadron collisions and hadron production. In 1960, the one-pion-exchange (OPE) model was first proposed [59,60] and then developed into a picture of peripheral interaction [61–63]. Difficulties at larger momentum transfers $-t$ led to replacement of one-particle exchange by exchange of Regge poles [63,64]. However, the Regge-pole exchange alone turned out also inadequate for the description of amplitudes. This discrepancy has been called absorption, and various absorption models have been studied phenomenologically [64–66,45], including the use of dispersion relations [67]. Our amplitude analysis provides direct experimental information on the production amplitudes, and thus it enables us to examine some of the models developed for the study of $\pi N \rightarrow \pi\pi N$ reactions. We will look separately at the momentum-transfer distribution in the ρ^0 mass region and at the mass dependence of amplitudes.

A. Dependence on t in ρ^0 mass region

A simple Regge model for the reaction $\pi^- p \rightarrow (\pi^- \pi^+) n$ with dipion mass confined to the ρ^0 mass interval was constructed by Kimel and Owens [44] to examine the role of “ A_1 ” exchange in data at 17.2 GeV/c for $-t=0-1.0$ (GeV/c)². Several structural features of the model can be tested by the results of our amplitude analysis without making any refit of the model’s many free parameters.

The model assumes that the S -wave nucleon helicity amplitudes S_0 and S_1 are proportional to the s -channel amplitudes L_0 and L_1 , respectively, as

$$S_n = \xi L_n, \quad \xi = P e^{i\Delta}, \quad n = 0, 1, \quad (5.1)$$

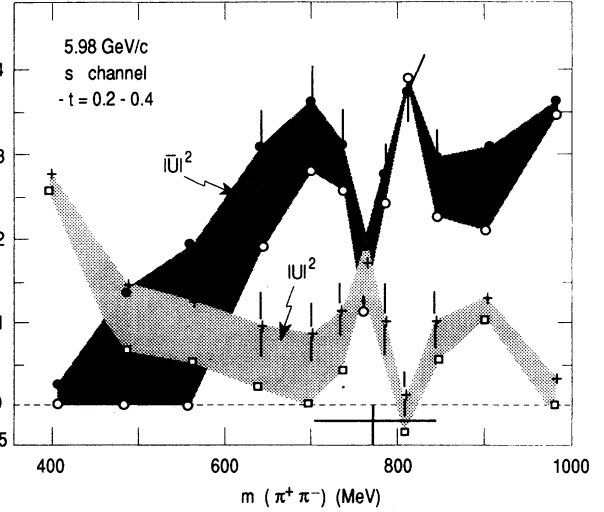
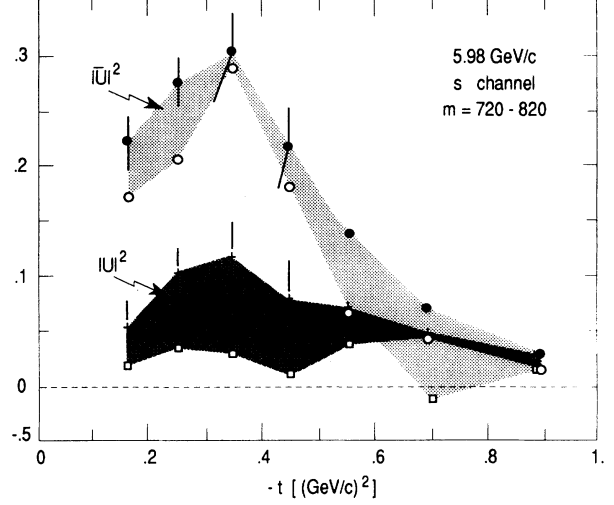


FIG. 13. The t dependence and the m dependence of lower and upper bounds with statistical errors for the amplitudes $|U|^2$ and $|\bar{U}|^2$ in the s channel at 5.98 GeV/c .

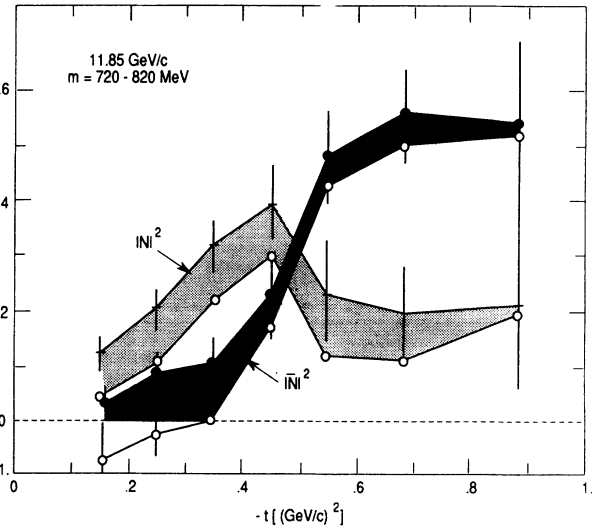


FIG. 14. The t dependence of lower and upper bounds with errors for amplitudes $|N|^2$ and $|\bar{N}|^2$ at 11.85 GeV/c . The amplitudes are helicity frame invariant.

where P and Δ are constants with values ≈ 0.4 . From (5.1) it follows that, in the s channel,

$$\begin{aligned} \cos(\gamma_{SL}) &= \cos(\bar{\gamma}_{SL}) = \cos(\Delta) = \text{const} , \\ \tau_S &= P^2 \tau_L . \end{aligned} \quad (5.2)$$

A comparison of (5.2) with Figs. 1–3 shows that the assumptions (5.1) are not well supported by experimental data. In particular, $\tau_S(1,2)$ has a larger magnitude than $\tau_L(1,2)$, and $\tau_S(2,1)$ is large for $-t=0.35$ (GeV/c)², while $\tau_L(2,1)$ is consistent with zero.

The natural exchange amplitudes are parametrized as

$$\begin{aligned} N_0 &= R(A_2) , \\ N_1 &= \sqrt{-t'} k N_0 + C , \end{aligned} \quad (5.3)$$

where $R(A_2)$ is an A_2 exchange Regge pole, C is a Regge cut contribution, and k is a constant. The relative phase of amplitudes N_0 and N_1 is given in terms of Regge trajectories α_{A_2} and α_c of the pole and the cut. Using the model's parametrization of these trajectories, we get, for the relative phase,

$$\phi_{N_0} - \phi_{N_1} = -\frac{\pi}{2}(\alpha_{A_2} - \alpha_c) = -\frac{\pi}{2}(0.43 + 0.34t) . \quad (5.4)$$

The partial-wave polarization

$$\tau_N = -2 \text{Im}(N_0 N_1^*) = 2|N_0| |C| \sin \frac{\pi}{2}(\alpha_{A_2} - \alpha_c) \quad (5.5)$$

is then predicted to be positive and changing sign at $-t \approx 1.27$. Data in Fig. 3 show that, while τ_N is positive at smaller t , it is changing sign already at $-t \approx 0.5$ (GeV/c)². This position of the zero of τ_N is close to the zero of the A_2 exchange trajectory $\alpha_{A_2} = 0.43 + 0.74t$ used in the model. This suggests that the natural exchange amplitudes N_0 and N_1 have a structure different from this model.

In the Kimel-Owens model, the nucleon helicity-flip amplitudes L_1 and U_1 in the s channel are dominated by a pion-exchange Regge pole with U_1 also receiving a Regge-cut contribution. The nonflip amplitudes L_0 and U_0 receive contributions from A_1 exchange Regge pole and a Regge cut. At 17.2 GeV/c, the model predicts $\tau_L < 0$ for $-t \leq 1.0$ (GeV/c)², while τ_U changes sign at $-t \approx 0.25$ (GeV/c)² and is positive for $-t \geq 0.25$ (GeV/c)². This result is in qualitative agreement with our amplitude analysis at 11.85 GeV/c (Fig. 2).

B. The mass dependence of amplitudes

The dependence of production amplitudes on the dipion invariant mass m is still little understood both experimentally and theoretically. Factorization of m dependence and t dependence has been commonly assumed in the study of $\pi N \rightarrow \pi\pi N$ and $KN \rightarrow K\pi N$ processes [66,68–70]. In our notation the assumption of factorization implies

$$H_{\lambda\lambda_p,0\lambda_n}^J(s,t,m) = f^J(m) G_{\lambda\lambda_p,0\lambda_n}^J(s,t,m) , \quad (5.6)$$

where $f^J(m)$ is proportional to partial-wave amplitude

with orbital momentum J in $\pi\pi$ elastic scattering and contains most of the m dependence. The helicity amplitudes $G_{\lambda\lambda_p,0\lambda_n}^J$ are assumed to be only weakly dependent on mass m at least in the resonance region. Using the relations (2.9) and (2.11) we obtain a similar factorization for our transversity amplitudes. For P -wave amplitudes $A = L, U, N$,

$$\begin{aligned} A(s,t,m) &= f^1(m) B(s,t,m) , \\ \bar{A}(s,t,m) &= f^1(m) \bar{B}(s,t,m) , \end{aligned} \quad (5.7)$$

where B and \bar{B} are formed from the amplitudes $G_{\lambda\lambda_p,0\lambda_n}^1$ using (2.9) and (2.11) and depend weakly on mass m . The mass dependence of moduli squared at fixed $-t$,

$$\begin{aligned} |A|^2 &= |f^1|^2 |B|^2 , \\ |\bar{A}|^2 &= |f^1|^2 |\bar{B}|^2 , \end{aligned} \quad (5.8)$$

is then determined by the common factor $|f^1|^2$. In particular, in the ρ^0 mass region, all P -wave moduli are expected to exhibit a similar resonant shape independent of $-t$.

This consequence of the factorization hypothesis is contradicted by the results of our amplitude analysis for the mass dependence of the moduli. As is seen in Figs. 5–8, the moduli do not have a uniform shape independent of nucleon transversity and meson helicity. For instance, at 5.98 GeV/c, the amplitude $|L|^2$ peaks while $|\bar{L}|^2$ dips at the resonant mass in the t channel. Moreover, elsewhere [38] we have shown that the shape of moduli squared within ρ^0 mass region changes with $-t$ dramatically (see also Fig. 15). We conclude that the factorization hypothesis is not well supported by the data on a polarized target. This conclusion casts some doubt on the previous studies of meson-meson scattering based on the extrapolation of unpolarized data on $\pi N \rightarrow \pi^+ \pi^- N$ into the unphysical region of t . The essential enabling assumption for the extraction of $\pi\pi$ phase shifts by this method was the factorization hypothesis (5.6).

C. The t evolution of mass dependence

The mass distribution of the spin-dependent moduli $|A|^2$ and $|\bar{A}|^2$ and the structures within the mass range of ρ^0 width vary with momentum transfer $-t$.

This conclusion is the result of our recent study [38] of the t evolution of mass dependence of bounds on the moduli squared in $\pi^+ n \rightarrow \pi^+ \pi^- p$ at 5.98 GeV/c. In this work we used Saclay data in an extended (m,t) binning covering the kinematic region:

$$360 \leq m \leq 920 \text{ MeV} \quad (5.9)$$

and

$$0.1 \leq -t \leq 1.0 \text{ (GeV/c)}^2$$

with six mass bins and the same seven t bins as in the binning (1.3). Additional results at 11.85 GeV/c are shown in Fig. 15.

In Ref. [38] and in Fig. 15 we present improved upper bounds obtained by introducing a nonlinear lower bound

on the S -wave moduli $|S|^2$ and $|\bar{S}|^2$. From (2.21b) we get, in each channel,

$$|S| \geq \frac{|a_5|}{|U|_{\text{upper}}} \quad \text{and} \quad |S| \geq \frac{|a_6|}{|L|_{\text{upper}}}, \quad (5.10)$$

where $|U|_{\text{upper}}$ and $|L|_{\text{upper}}$ are given by (4.6). We now define a lower bound on $|S|$ as

$$|S|_{\text{lower}} = \min_{s \text{ and } t} \left\{ \frac{|a_5|}{|U|_{\text{upper}}}, \frac{|a_6|}{|L|_{\text{upper}}} \right\}. \quad (5.11)$$

The new upper bounds for moduli squared of P -wave amplitudes $A = L, U, \bar{N}$ then are

$$|A|_{\text{upper}}^2 = (|A|^2 + \frac{1}{3}|S|^2) - \frac{1}{3}|S|_{\text{lower}}^2. \quad (5.12)$$

The lower bound $|\bar{S}|_{\text{lower}}$ and the new upper bounds on the moduli of amplitudes $\bar{L}, \bar{U}, \bar{N}$ are obtained similarly. The lower bounds (4.9) on P -wave moduli were left unchanged.

We note that the ρ_0 resonance peak is seen in the reaction cross section $d^2\sigma/dm dt \equiv \Sigma$ at all measured momentum transfers. The observed structures near resonance masses and their change with $-t$ indicate that the resonant peak in Σ is not uniformly copied on the level of unnormalized amplitudes $|A|^2\Sigma$ and $|\bar{A}|^2\Sigma$. Instead, the t -dependent structures within the resonance width provide entirely new and nontrivial information about the dynamics of ρ^0 resonance production.

D. Possible effects of hadron structure

The t dependence of moduli $|N|^2$ and $|\bar{N}|^2$ in the ρ^0 mass region shows a clear crossover of these moduli at $-t_c = 0.4-0.5$ (GeV/c)² at both incident momenta. In contrast, the CERN-Munich amplitude analysis [13,14] of $\pi^- p \rightarrow \pi^- \pi^+ n$ at 17.2 GeV/c shows no crossover of $|N|^2$ and $|\bar{N}|^2$ at these values of $-t$. There is a possible crossover at $-t_c = 0.7-0.8$ (GeV/c)². The quality of both experiments suggests that the observed difference is a real effect. The difference in t_c could be due to energy dependence of the crossover point t_c or it could be an energy-independent feature of natural exchange amplitudes. Only new experiments can distinguish between these two possibilities. We suggest one consider the observed difference in the position of crossover in the amplitudes $|N|^2$ and $|\bar{N}|^2$ as a signal of the influence of hadron composite structure in hadron production processes [71,72].

The expectation that the behavior of natural exchange amplitudes should be the same in both reactions originates in a simplified view of Regge poles and Regge cuts developed in 1960s. It was recognized already then that Regge poles reflect the composite structure of exchanged objects and that Regge cuts arise from the composite structure of colliding hadrons and from the spatiotemporal ordering of hadron breakup and reintegration during scattering [71,72]. But, in practice, this nature of Regge singularities was sidestepped in Regge models and Regge phenomenology. Regge poles were coupled to elementary hadrons in Feynman-like diagrams with factorizable vertices. The Regge cuts were modeled either by multiple scattering of elementary hadrons in the initial and the final states of interactions, or by the multiple exchange of Regge poles between elementary hadrons. In such Regge models, the reactions $\pi^+ n \rightarrow \pi^+ \pi^- p$ and $\pi^- p \rightarrow \pi^- \pi^+ n$ are described by exchange diagrams with the same Regge poles and the amplitudes in both reactions show the same structure. Any departure from this expectation suggests one reconsider the neglect of the

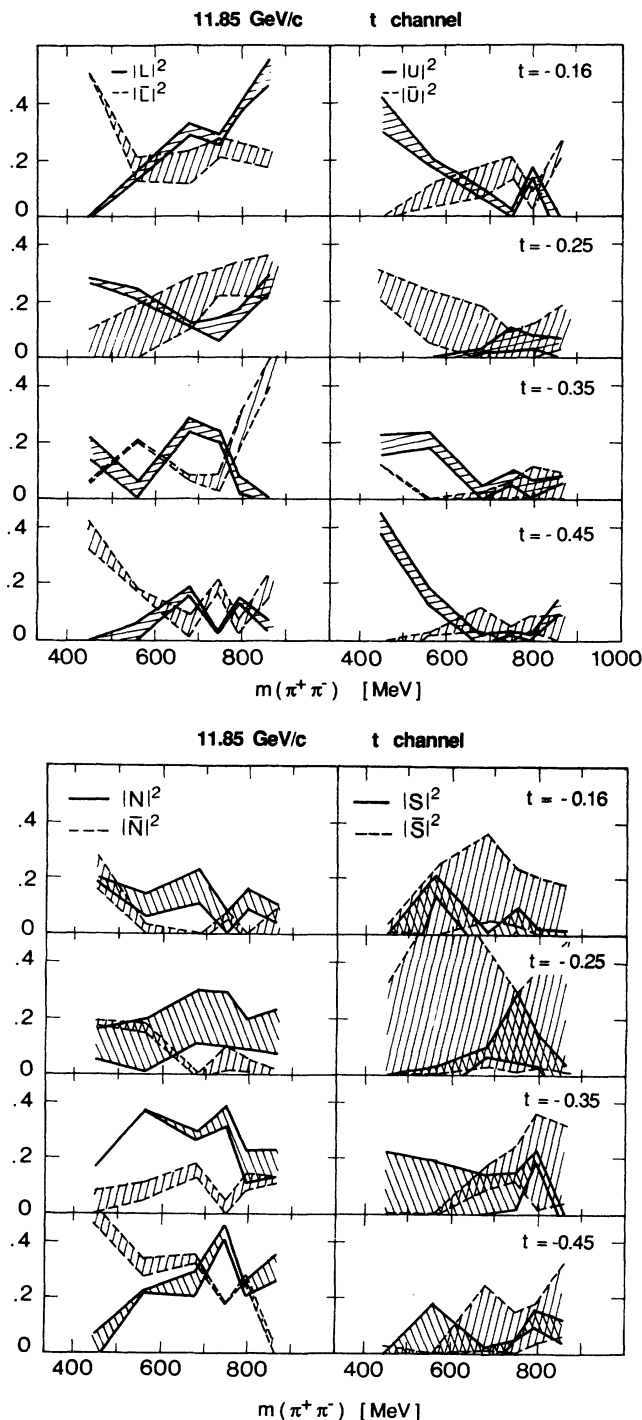


FIG. 15. The t evolution of mass dependence of moduli squared of t -channel normalized nucleon transversity amplitudes at 11.85 GeV/c . (Results at 5.98 GeV/c are presented in Ref. [38].)

composite nature of hadrons and exchanged objects in the modeling of Regge singularities and scattering amplitudes.

In principle, the hadron structure and interactions at small t are described by nonperturbative quantum chromodynamics (QCD). QCD provides a physical basis for the interpretation of Regge singularities and introduces non- $q\bar{q}$ exchanges. Deviations from simple Regge models found in experimentally determined amplitudes can thus be viewed as manifestations of nonperturbative QCD effects.

VI. SUMMARY

We have performed a model-independent amplitude analysis of the reaction $\pi^+ n_{\uparrow} \rightarrow \pi^+ \pi^- p$ at 5.98 and 11.85 GeV/ c using Saclay data in two sets of binnings (1.3) and (1.4) to study the t dependence of pion production amplitudes in the ρ^0 mass region and their mass dependence below 1000 MeV for $-t = 0.2-0.4$ (GeV/ c)². The data on a transversely polarized target are best analyzed in terms of normalized nucleon transversity amplitudes (NTA's). In our kinematic region we worked with two S -wave and six P -wave amplitudes in both s - and t -channel dipion helicity frames.

Our analysis yields in each (m, t) bin two solutions for eight moduli and six cosines of relative phases between pairs of amplitudes (3.3). The two solutions are similar with the largest difference being in the S -wave moduli. In some (m, t) bins the analysis leads to unphysical complex moduli. In such cases we presented their real parts. This procedure is justified since the imaginary parts are relatively small and the real parts are within the linear bounds (4.6) and (4.9). The occurrence of unphysical values of moduli and cosines is very likely due to the use of unconstrained optimization of the maximum-likelihood function in the data analysis. We suggest that future experiments use a constrained optimization in their data analysis.

We presented a detailed description of the behavior of amplitudes which show new and important features both in their t dependence and m dependence. Both solutions require nonzero nucleon helicity-nonflip amplitudes (“ A_1 ” exchange) with phases different from the phases of nucleon helicity-flip amplitudes (“ π ” exchange). This result confirms the previous evidence for “ A_1 ” exchange found in the CERN-Munich amplitude analysis of $\pi^- p_{\uparrow} \rightarrow \pi^- \pi^+ n$ at 17.2 GeV/ c .

The t dependence of natural exchange amplitudes $|N|^2$ and $|\bar{N}|^2$ shows a crossover at $-t_c = 0.4-0.5$ (GeV/ c)² at both energies. The CERN-Munich analysis shows no crossover in the “ A_2 ” exchange amplitudes $|N|^2$ and $|\bar{N}|^2$ at this value of $-t$. We suggest that this difference may be a real effect associated with the composite structure of hadrons [72].

From a comparison of our results with the Regge model of Kimel-Owens, we concluded that the experimentally determined amplitudes S, \bar{S} and N, \bar{N} have structures different from the assumptions made about these amplitudes in this model. The differences in mass dependence of the moduli squares $|A|^2$ and $|\bar{A}|^2$, $A = S, L, U, N$, reflect an important role of nucleon spin in the pion

creation process. Particularly noteworthy are structures in the ρ^0 mass region seen in the amplitudes $|N|^2$, $|\bar{N}|^2$, $|L|^2$, and $|\bar{L}|^2$ (t channel) and $|U|^2$ and $|\bar{U}|^2$ (s channel) and their t evolution (Fig. 15 and Ref. [38]). We concluded that the ρ^0 peak seen in $d^2\sigma/dm dt$ and in the smooth partial-wave cross sections (Fig. 10) is not uniformly copied on the level of amplitudes. We suggest that the structures in moduli within the ρ^0 mass region provide entirely new information on the dynamics of ρ^0 production. We also note that, in Fig. 10, the width of the ρ^0 peak in the natural exchange partial-wave cross section I_N is narrower in comparison with the ρ^0 peaks in the unnatural exchange partial-wave cross sections I_L and I_U .

The S -wave cross section shows a peak around 750 MeV, in particular in the solution $I_S(2,2)$. This behavior of I_S suggests that the possibility of the existence of a scalar state $I = 00^{++}(750)$ should be considered. We will discuss in detail this aspect of our amplitude analysis elsewhere. The observed features of mass dependence of P -wave moduli squared do not support the hypothesis of factorization of mass and momentum-transfer dependence in pion production amplitudes previously used in studies of meson-meson scattering.

To conclude, we have demonstrated that new and important information on hadron dynamics and properties of hadron resonances is provided by amplitude analysis of the pion production processes $\pi N \rightarrow \pi\pi N$. Our results warrant new efforts to reach the level of amplitudes experimentally and with a high degree of precision in a new generation of experiments with spin at the recently proposed advanced hadron facilities [73–83].

ACKNOWLEDGMENTS

This work was supported by Fonds pour la Formation de Chercheurs et l'Aide à la Recherche (FCAR), Ministère de l'Éducation du Québec, Canada, and by Commissariat à l'Énergie Atomique, Saclay, France.

APPENDIX

Calculation of phases γ_{NS} and $\bar{\gamma}_{NS}$

In this appendix we solve Eqs. (2.23) for the helicity frame invariant relative phases $\gamma_{NS} = \phi_N - \phi_S$ and $\bar{\gamma}_{NS} = \bar{\phi}_N - \bar{\phi}_S$. Other phases in (2.23) are then expressed in terms of these phases and phases (3.3):

$$\begin{aligned} \gamma_{NU} &= \phi_N - \phi_U = (\phi_N - \phi_S) + (\phi_S - \phi_U) = \gamma_{NS} - \gamma_{US}, \\ \gamma_{NL} &= \phi_N - \phi_L = (\phi_N - \phi_S) + (\phi_S - \phi_L) = \gamma_{NS} - \gamma_{LS}, \end{aligned} \quad (\text{A1})$$

with similar relations for $\bar{\gamma}_{NU}$ and $\bar{\gamma}_{NL}$. The system of equations (2.23) can then be written as

$$\begin{aligned} b_1 &= |N||U|\cos(\gamma_{NS} - \gamma_{US}) - |\bar{N}||\bar{U}|\cos(\bar{\gamma}_{NS} - \bar{\gamma}_{US}), \\ b_2 &= |N||L|\cos(\gamma_{NS} - \gamma_{LS}) - |\bar{N}||\bar{L}|\cos(\bar{\gamma}_{NS} - \bar{\gamma}_{LS}), \\ b_3 &= |N||S|\cos(\gamma_{NS}) - |\bar{N}||\bar{S}|\cos(\bar{\gamma}_{NS}). \end{aligned} \quad (\text{A2})$$

From b_3 we obtain

$$\cos\bar{\gamma}_{NS} = \frac{|N||S|\cos\gamma_{NS} - b_3}{|\bar{N}||\bar{S}|} \quad (\text{A3})$$

and from b_2 we have

$$\sin \bar{\gamma}_{NS} = -\cos \bar{\gamma}_{NS} (\cos \bar{\gamma}_{LS} / \sin \bar{\gamma}_{LS}) + \frac{b_2 - |N||L|(\cos \gamma_{NS} \cos \gamma_{LS} + \sin \gamma_{NS} \sin \gamma_{LS})}{|\bar{N}||\bar{L}|\sin(\bar{\gamma}_{LS})}. \quad (\text{A4})$$

We now define

$$\begin{aligned} c_1 &\equiv |L||S|\sin \gamma_{LS} = \epsilon_1 \sqrt{|L|^2|S|^2 - a_6^2}, \\ c_2 &\equiv |U||S|\sin \gamma_{US} = \epsilon_2 \sqrt{|U|^2|S|^2 - a_5^2}, \\ c_3 &\equiv |U||L|\sin \gamma_{UL} = \epsilon_3 \sqrt{|U|^2|L|^2 - a_4^2}, \end{aligned} \quad (\text{A5})$$

where $\epsilon_k = \pm 1$, $k = 1, 2, 3$ is the sign ambiguity of the sines. The c_3 and the sign ϵ_3 are not independent of c_1 and c_2 :

$$|S|^2 c_3 = a_6 c_2 - a_5 c_1. \quad (\text{A6})$$

Similarly we define \bar{c}_1 , \bar{c}_2 , and \bar{c}_3 for amplitudes with opposite transversity. Substituting from (A3) and from (A4) into the equation for b_1 and using the above definitions for c_k , \bar{c}_k , $k = 1, 2, 3$, we obtain

$$(b_1 \bar{c}_1 + b_2 \bar{c}_2 + b_3 \bar{c}_3) |\bar{S}|^2 |S| = \sin \gamma_{NS} |N| |\bar{S}|^2 (c_1 \bar{c}_2 + \bar{c}_1 c_2) + \cos \gamma_{NS} |N| \{ \bar{c}_1 (a_5 |\bar{S}|^2 - \bar{a}_5 |S|^2) + \bar{c}_2 (a_6 |\bar{S}|^2 + \bar{a}_6 |S|^2) \}. \quad (\text{A7})$$

We now define

$$\begin{aligned} d &= \frac{b_1 \bar{c}_1 + b_2 \bar{c}_2 + b_3 \bar{c}_3}{c_1 \bar{c}_2 + \bar{c}_1 c_2} \left[\frac{|S|}{|N|} \right], \\ \tan \alpha &= \frac{\bar{c}_1 (a_5 |\bar{S}|^2 - \bar{a}_5 |S|^2) + \bar{c}_2 (a_6 |\bar{S}|^2 + \bar{a}_6 |S|^2)}{(c_1 \bar{c}_2 + \bar{c}_1 c_2) |\bar{S}|^2}. \end{aligned} \quad (\text{A8})$$

With this notation (A7) takes the form

$$\sin \gamma_{NS} + \cos \gamma_{NS} \tan \alpha = d. \quad (\text{A9})$$

Its solution is

$$\begin{aligned} \cos \gamma_{NS} &= \frac{1}{1 + \tan^2 \alpha} \{ d \tan \alpha \pm \sqrt{1 + \tan^2 \alpha - d^2} \}, \\ \sin \gamma_{NS} &= \frac{1}{1 + \tan^2 \alpha} \{ d \mp \tan \alpha \sqrt{1 + \tan^2 \alpha - d^2} \}. \end{aligned} \quad (\text{A10})$$

Using (A10) we obtain $\cos \bar{\gamma}_{NS}$ and $\sin \bar{\gamma}_{NS}$ from (A3) and (A4).

There are four combinations of solutions for moduli $|A|^2$, $|\bar{A}|^2$, $A = S, L, U, N$ entering the calculation of d and $\tan \alpha$. In addition, each such combination is accompanied by the fourfold sign ambiguity from the undetermined signs ϵ_k and $\bar{\epsilon}_k$, $k = 1, 2$. This 16-fold ambiguity increases to 32-fold ambiguity due to sign ambiguity in (A10).

The solvability of (A9) imposes a nonlinear constraint on data and on the solutions for moduli squared

$$d^2 - 1 \leq \tan^2 \alpha. \quad (\text{A11})$$

Additional constraints follow from the requirement that cosines and sines of γ_{NS} and $\bar{\gamma}_{NS}$ have physical values. In principle, these constraints could reduce the overall ambiguity of solution (A10).

-
- [1] H. A. Bethe, *Ann. Phys. (N.Y.)* **3**, 190 (1958).
[2] E. R. Schumacher and H. A. Bethe, *Phys. Rev.* **121**, 1534 (1961).
[3] F. Halzen and C. Michael, *Phys. Lett.* **36B**, 367 (1971).
[4] R. L. Kelly, *Phys. Lett.* **39B**, 635 (1972).
[5] G. Cozzika *et al.*, *Phys. Lett.* **40B**, 281 (1972).
[6] R. C. Miller, A. Yokosawa, and P. Johnson, *Nuovo Cimento* **22A**, 99 (1974).
[7] M. Svec *et al.*, *High Energy Physics with Polarized Beams and Polarized Targets (Argonne, 1978)*, Proceedings of the Third International Symposium, edited by G. H. Thomas, AIP Conf. Proc. No. 51 (AIP, New York, 1979), p. 491.
[8] M. Fujisaki *et al.*, *Nucl. Phys.* **B152**, 232 (1979).
[9] P. W. Johnson and G. M. Thomas, *Phys. Rev. D* **16**, 2783 (1977).
[10] I. P. Auer *et al.*, *Phys. Rev. D* **32**, 1609 (1985).
[11] G. R. Goldstein *et al.*, *Nucl. Phys.* **B80**, 164 (1974).
[12] J. Bystricky, F. Lehar, P. Winternitz, *J. Phys. (Paris)* **39**, 1 (1978); **45**, 207 (1984).
[13] P. La France and P. Winternitz, *J. Phys. (Paris)* **41**, 1391 (1980).
[14] G. R. Goldstein and M. J. Moravcsik, *Ann. Phys. (N.Y.)* **142**, 219 (1982).
[15] J. K. Gottfried and J. D. Jackson, *Nuovo Cimento* **33**, 309 (1964).
[16] G. Lutz and K. Rybicky, Max Planck Institute, Munich, Internal Report No. MPI-PAE/Exp. EI.75, 1978 (unpublished).
[17] J. G. M. de Groot, Ph.D. thesis, Universiteit van Amsterdam, 1978.
[18] H. Becker *et al.*, *Nucl. Phys.* **B150**, 301 (1979).
[19] H. Becker *et al.*, *Nucl. Phys.* **B151**, 46 (1979).
[20] V. Chabaud *et al.*, *Nucl. Phys.* **B223**, 1 (1983).
[21] I. Sakrejda, Ph.D. thesis, Institute of Nuclear Physics, Cracow, 1984.
[22] K. Rybicky and I. Sakrejda, *Z. Phys. C* **28**, 65 (1985).
[23] K. Rybicky, I. Sakrejda, and J. Turnau, *Acta Phys. Pol.* **B17**, 317 (1986).
[24] M. Blackman and G. R. Goldstein, *Phys. Rev. D* **1**, 2675 (1970).

- [25] M. Babou *et al.*, Nucl. Instrum. Methods **160**, 1 (1979).
- [26] A. de Lesquen *et al.*, in *Low and Intermediate Energy Kaon-Nucleon Physics*, Proceedings of the Workshop, Rome, Italy, 1980, edited by E. Ferrari and G. Violini (Reidel, Dordrecht, 1981), p. 289.
- [27] A. Itano *et al.*, in *High Energy Physics with Polarized Beams and Targets*, edited by C. Joseph and J. Soffer (Birkhauser, Boston, 1981), p. 560.
- [28] A. de Lesquen *et al.*, CEN-Saclay Internal Report DPhPE No. 82-01, 1982 (unpublished), pp. 1–56.
- [29] A. de Lesquen *et al.*, Phys. Rev. D **32**, 21 (1985).
- [30] Particle Data Group, A. de Lesquen *et al.*, Record ID-4023, Rutherford Laboratory, England, 1986 (unpublished).
- [31] A. de Lesquen *et al.*, Phys. Rev. D **39**, 21 (1989).
- [32] M. Svec *et al.*, in *Low and Intermediate Energy Kaon-Nucleon Physics* [26], p. 305.
- [33] M. Svec *et al.*, in *High Energy Physics with Polarized Beams and Targets* [27], p. 566.
- [34] A. de Lesquen *et al.*, CEN-Saclay Internal Report DPhPE No. 82-01, 1982 (unpublished), pp. 87–110.
- [35] M. Svec, J. Phys. (Paris) Colloq. **46**, C-281 (1985).
- [36] M. Svec, in *Hadron Spectroscopy—1985*, Proceedings of the International Conference, College Park, Maryland, edited by S. Oneda, AIP Conf. Proc. No. 132 (AIP, New York, 1985), p. 68.
- [37] M. Svec, A. de Lesquen, and L. van Rossum, in *Intersections Between Particle and Nuclear Physics*, Lake Louise, Canada, 1986, Proceedings of the Second Conference, edited by Donald F. Geesman, AIP Conf. Proc. No. 150 (AIP, New York, 1986), p. 1198.
- [38] M. Svec, A. de Lesquen, and L. van Rossum, Phys. Rev. D **42**, 934 (1990).
- [39] E. Byckling and K. Kajantie, *Particle Kinematics* (Wiley, New York, 1973).
- [40] S. Humble, *Introduction to Particle Production of Hadrons* (Academic, New York, 1974).
- [41] R. Saenger and W. Schmidt, Ann. Phys. (N.Y.) **54**, 307 (1969).
- [42] R. J. Cashmore, in *Phenomenology of Particles at High Energies*, 14th Scottish Universities Summer School in Physics, 1973, edited by R. L. Crawford and R. Jennings (Academic, New York, 1974), p. 611.
- [43] D. B. Ion and C. Mihul, Ann. Phys. (N.Y.) **83**, 41 (1975).
- [44] J. D. Kimel and J. F. Owens, Nucl. Phys. **B122**, 469 (1977).
- [45] C. Bourrely, E. Leader, and J. Soffer, Phys. Rep. **59**, 95 (1980).
- [46] A. Kotanski, Acta Phys. Pol. **29**, 699 (1966); **30**, 629 (1966); **B1**, 45 (1970).
- [47] G. Cohen-Tannoudji *et al.*, Ann. Phys. (N.Y.) **46**, 239 (1968).
- [48] F. D. Gault, G. R. Goldstein, and H. F. Jones, Nuovo Cimento **27A**, 174 (1975).
- [49] P. J. Bussey *et al.*, Nucl. Phys. **B154**, 205 (1980).
- [50] I. I. Bronshtein and K. A. Semendyayev, *Handbook of Mathematics* (Gosudarstvennoe Izdatelstvo Tekhniko-Teoreticheskoi Literatury, Moscow, 1954), p. 139.
- [51] M. Svec (unpublished).
- [52] M. Svec, A. de Lesquen, and L. van Rossum, Phys. Lett. B **220**, 653 (1989).
- [53] Ph. E. Gill, W. Murray, and M. M. Wright, *Practical Optimization* (Academic, New York, 1981).
- [54] S. S. Rao, *Optimization and Applications* (Wiley, New York, 1984), p. 723.
- [55] B. A. Murtagh and M. A. Saunders, MINOS 5.0 Users Guide, Systems Optimization Laboratory Report No. SOL 83-20, Stanford University, 1983 (unpublished).
- [56] I. Siline, CERN Computer Center Program Library, Report No. D510, 1971 (unpublished).
- [57] P. Bonamy *et al.*, Nucl. Phys. **B52**, 392 (1973).
- [58] G. Girardi *et al.*, Nucl. Phys. **B76**, 541 (1974).
- [59] S. D. Drell, Phys. Rev. Lett. **5**, 342 (1960).
- [60] F. Salzman and G. Salzman, Phys. Rev. **120**, 599 (1960).
- [61] J. D. Jackson, Rev. Mod. Phys. **37**, 484 (1965).
- [62] J. D. Jackson, in *High Energy Physics*, Proceedings of the Les Houches Summer School of Theoretical Physics, Les Houches, France, 1965 (Gordon and Breach, New York, 1965), p. 369.
- [63] S. Gasiorowicz, *Elementary Particle Physics* (Wiley, New York, 1966).
- [64] P. D. B. Collins, Phys. Rep. C **1**, 103 (1971).
- [65] A. C. Irving and R. P. Worden, Phys. Rep. **34**, 117 (1977).
- [66] A. B. Wicklund *et al.*, Phys. Rev. **17**, 1197 (1978).
- [67] M. Svec, Phys. Rev. D **22**, 70 (1980).
- [68] P. E. Schlein, Phys. Rev. Lett. **19**, 1052 (1967).
- [69] P. Estabrooks *et al.*, in π - π Scattering, Proceedings of the Tallahassee Conference, edited by D. K. Williams and V. Hagopian, AIP Conf. Proc. No. 13 (AIP, New York, 1973).
- [70] P. Estabrooks *et al.*, Nucl. Phys. **B133**, 490 (1978).
- [71] F. Henyey, G. L. Kane, J. Pumplin, and M. M. Ross, Phys. Rev. **182**, 1579 (1969).
- [72] P. D. B. Collins, Nucl. Phys. **B52**, 165 (1973).
- [73] E. Vogt, Nucl. Phys. **A450**, 453c (1986); J. Domingo, *ibid.* **A450**, 473c (1986); G. T. Garvey, *ibid.* **A450**, 539c (1986).
- [74] *Canadian Kaon Factory* (TRIUMF, Vancouver, 1985).
- [75] Physics and A plan for a 45 GeV Facility, LANL Report No. LA-10720-MS, Los Alamos, 1986 (unpublished).
- [76] *Proceedings of the International Conference on a European Hadron Facility*, Mainz, Germany, 1986, edited by T. Walcher [Nucl. Phys. **B279**, 2 (1987)].
- [77] *International Workshop on Hadron Facility Technology*, Proceedings, Los Alamos, New Mexico, 1987, edited by H. A. Thiessen (LANL Report No. LA-11130-C, Los Alamos, 1987).
- [78] Japanese Hadron Facility, in *International Workshop on Hadron Facility Technology* [77], p. 67.
- [79] *Physics at KAON*, edited by D. Frekers, D. R. Gill, and J. Speth (Springer-Verlag, Berlin, 1990) [Z. Phys. C **46**, S1 (1990)].
- [80] *Multiuser Hadron Spectrometer Workshop*, edited by M. Comyn (TRIUMF, Vancouver, 1990).
- [81] *Workshop on Science at KAON*, edited by M. Comyn and D. R. Gill (TRIUMF, Vancouver, 1990).
- [82] G. Preparata, in *Intense Hadron Facilities and Antiproton Physics*, Proceedings of the Conference, edited by T. Bresnani, F. Iazzi, and G. Pauli (Societa Italiana di Fisica, Bologna, Italy, 1990), Vol. 26.
- [83] M. Svec, *High-Energy Spin Physics: Eighth International Symposium*, Proceedings of the Eighth International Symposium, edited by Kenneth J. Heller, AIP Conf. Proc. No. 187 (AIP, New York, 1989), Vol. 2, p. 1181.

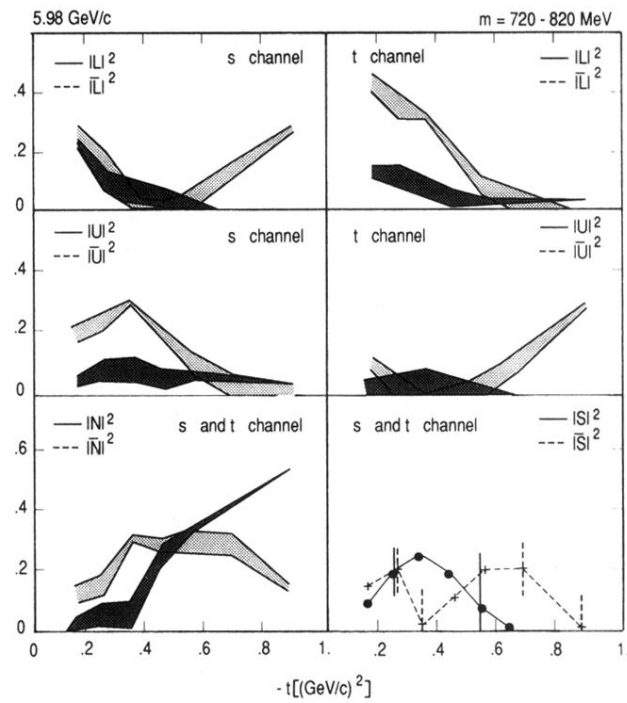


FIG. 11. The t dependence of the lower and upper bounds on the moduli squared of the normalized P -wave nucleon transversity amplitudes for $m = 720\text{--}820$ MeV at 5.98 GeV/ c . Also shown are the upper bounds for the normalized S -wave amplitudes.

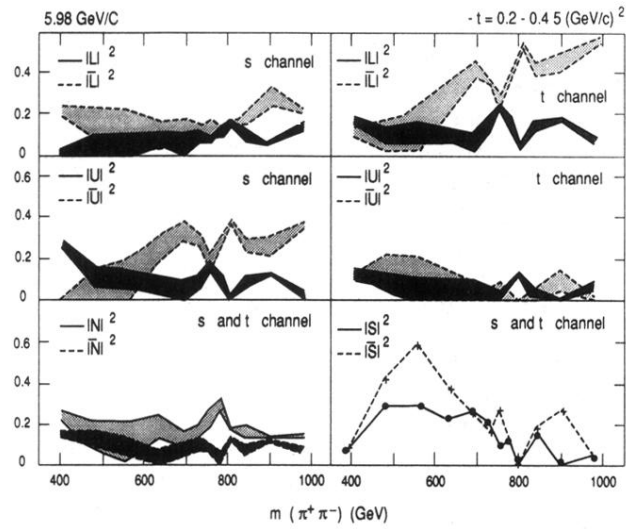


FIG. 12. The m dependence of the lower and upper bounds on the moduli squared of the normalized P -wave nucleon transversity amplitudes for $-t=0.2-0.4 \text{ (GeV/c)}^2$ at 5.98 GeV/c , and the upper bounds for the S -wave normalized moduli squared.

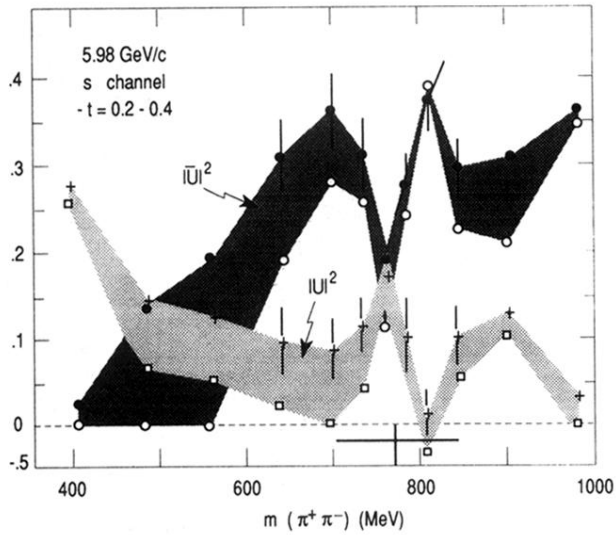
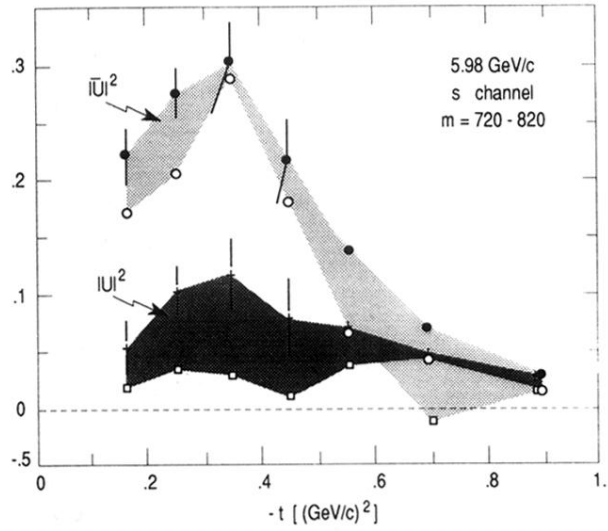


FIG. 13. The t dependence and the m dependence of lower and upper bounds with statistical errors for the amplitudes $|U|^2$ and $|\bar{U}|^2$ in the s channel at $5.98 \text{ GeV}/c$.

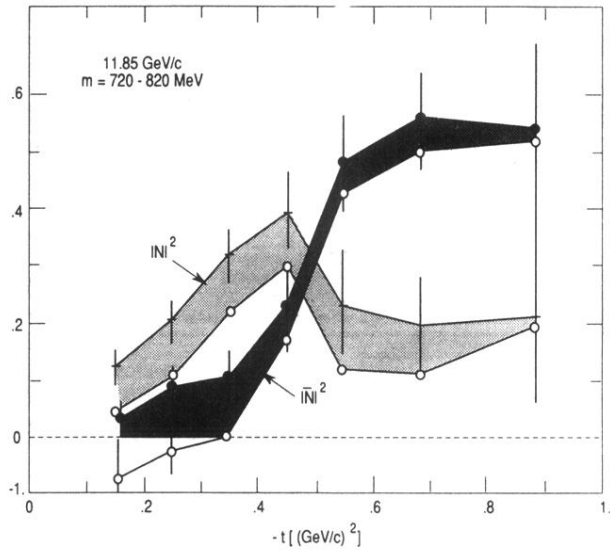


FIG. 14. The t dependence of lower and upper bounds with errors for amplitudes $|N|^2$ and $|\bar{N}|^2$ at 11.85 GeV/c. The amplitudes are helicity frame invariant.